REAL-TIME COMPARISONS OF IONOSPHERIC DATA

WITH OUTPUTS FROM THE UAF EULERIAN

PARALLEL POLAR IONOSPHERE MODEL.

By

Nagaprasad V. Kotipalli

RECOMMENDED:

Advisory Committee Chair

Head, Department of Electrical and Computer Engineering

APPROVED:

Dean, College of Engineering and Mines

Dean of the Graduate School

April 6, 2007

Date

REAL-TIME COMPARISONS OF IONOSPHERIC DATA WITH OUTPUTS FROM THE UAF EULERIAN PARALLEL POLAR IONOSPHERE MODEL

A

THESIS

Presented to the Faculty

of the University of Alaska Fairbanks

in Partial Fulfillment of the Requirements

for the Degree of

MASTER OF SCIENCE

By

Nagaprasad V. Kotipalli

Fairbanks, Alaska

May 2007

ABSTRACT

The UAF theoretical polar ionospheric model (UAF EPPIM) solves 3D equations of mass, momentum, and energy balance for multiple ion species to determine ion and electron parameters in the polar ionosphere region using a parallel numerical code on an Eulerian grid. Real time operation of the model is very important because users are interested in current space weather conditions. Real-time validation of this model with available experimental data is an important task for the following reasons. (1) Real-time validation can provide much information about the model quality and define the directions of improvement. (2) Real-time comparisons help to determine trusted intervals for the model parameters for future data assimilation tasks. In this work, we have developed an operational real-time comparisons capability which assimilates HAARP (High frequency Active Auroral Research Program) experimental data for the model validation purposes. Software has been developed to emulate Total Electron Content (TEC). Results are then compared with real-time data from HAARP. Further, we have developed a Computerized Ionospheric Tomography (CIT) model which provides ionosphere tomography images covering five different stations in Alaska along the geomagnetic latitude (50-78 degrees). Then these images are compared with real-time ionosphere tomography images obtained at the HAARP website.

Table of Contents

Page

Page

Page

Page

Page

List of Figures

Page

List of Tables

Page

Acknowledgements

I really thank my advisor Dr. Brenton Watkins for giving me this opportunity to work on this project. His constant support and guidance helped me a lot in completing this thesis.

I would like to thank my supervisor and committee member Dr. Sergei Maurits, his leadership, support, encouragement and daily involvement helped in successful completion of my work. His constant involvement in the programming helped me learn good programming skills.

I also wish to express my gratitude to my committee member Dr. Vikas Sonwalkar. I can say my experience working as a teaching assistant to him helped me learn organization skills and maturity to survive in this competitive world. His timely advice proved to be valuable for me. I also would like to thank Dr. Anton Kulchisky for his support in development of the ionospheric tomography comparisons software. His excellent guidance in Python programming helped me in development of software for this thesis.

I would like to thank my parents for providing me support and encouragement to study for a Master's degree at UAF. My friends and fellow graduate students here at UAF were wonderful during my stay here in Fairbanks.

Last but not the least; I would like to thank Arctic Region Supercomputing Center for providing me funding to work on this project. ARSC also provided me with excellent computing resources which were very essential for this thesis. The staff and students here at ARSC were always cooperative and friendly to me. Finally it's the involvement and constant support of Sergei that made it possible for me to complete this thesis successfully.

Chapter 1 Introduction

1.1 Introduction to the Thesis

The ionosphere extends from about 80 km to many hundreds of kilometers in altitude. It is important for its effect on radio waves and the transmission of electromagnetic waves by satellite-based navigation systems such as the Global Positioning System (GPS) as they pass through the ionosphere. GPS radio signals are slowed down as they propagate through the ionosphere, causing an increase in the propagation time of a signal when compared to the time of propagation through free space. This propagation delay must be taken into account when determining position using the GPS system. The ionosphere is a dispersive medium, and since the dispersion changes with frequency in a known way, a dual frequency receiver can be used to effectively eliminate this propagation delay of GPS signals caused by the ionosphere and so provide highly accurate determinations of the position of receivers monitoring GPS, or other satellite navigation systems. However, because of their relative simplicity, single frequency GPS receiver systems are often used even though they have no possibility of measuring the ionospheric delay. Instead, ionospheric models must be relied on to provide the necessary correction for the ionospheric delay. Ionospheric models generally only represent average conditions and are mostly based on ionosonde measurements that only probe the bottom side of the ionosphere, i.e. the region below the maximum electron density which generally occurs in the range of 250 – 400 km altitude. Consequently it is important that the ability to model the ionosphere, including the topside ionosphere, is

improved for GPS applications. In fact, GPS observations can themselves be used to determine properties of the ionosphere. The signal propagation delay, or position correction, is proportional to the line integral of the free electron distribution along the path of the signal from the satellite transmitter to the receiver. The electron density distribution in the Earth's ionosphere as determined from a model can be used not only to correct for the propagation delay in GPS signals, but also to study the behavior of the ionosphere. For example, changes occurring during ionospheric storms, ion composition changes, and space-weather effects on telecommunications are just a few of the phenomena that can be studied.

The ionosphere delay that affects GPS signals may also be used to determine the TEC (Total Electron Content) of the ionosphere along a path from the GPS satellites to the ground station. TEC measurements, made using ionospheric radio signals, are one of the most important methods of investigating the Earth's ionosphere. However, by themselves, a series of TEC measurements are just a collection of line integrals of the electron density and only show the bulk behavior and structure of the ionosphere.

The primary aim of this thesis is to develop software tools to validate the UAF Polar Ionospheric Model through comparisons of GPS and other data. The UAF theoretical polar ionospheric model (UAF EPPIM) solves 3D equations of mass, momentum, and energy balance for multiple ion species to determine ion and electron parameters in the polar ionosphere region using a parallel numerical code on an Eulerian

grid. The model supports past analysis mode and also operates in real time. Real time operation of the model is very important because users are interested in current space weather conditions. A real-time updated forecast of ionospheric parameters is obtained every five minutes. Interaction with data in real-time allows for development of long term adaptive forecasting schemes in the long run. This effort is the first stage in this direction. Real-time validation of this model with available experimental data is an important task for the following reasons. (1) Real-time validation can provide much information about the model quality, determine its limitations and define the directions for improvement. (2) Real-time comparisons help to determine trusted intervals for the model parameters for future data assimilation tasks. In this case real-time comparisons are of forecast model capability.

The primary objective of this work is to develop an operational real time comparisons capability which assimilates experimental data for model validation purposes. Total Electron Content (TEC), TEC tomography data and Scintillation Index (S_4) from the Alaskan HARRP online depository have been utilized. HAARP (**H**igh frequency **A**ctive **A**uroral **R**esearch **P**rogram) is a major Arctic facility for upper atmospheric and solar-terrestrial research. The HAARP facility provides access to various types of ionospheric data like TEC tomography data, GPS TEC measurements and Scintillation Parameters.

This thesis contains six chapters. Chapter 1 is the basic introduction to this thesis, In Chapter 2, Introduction to Coordinate Systems, coordinate system conversions and azimuth and elevation angle derivations used in this project are described. Chapter 3 gives an overview of the ionosphere and especially the phenomena that influence the electron density distribution of the ionosphere. A brief history of the discovery of the ionosphere is also given. Chapter 4 is devoted to the emulation of ionospheric characteristics like Total Electron Content and Scintillation Index using GPS satellite data. Here the background history of both GPS satellites and their data format are briefly described. The GPS TEC reduction principles are described here in more detail. In Chapter 5, the ionospheric tomography method is outlined and comparisons are done between the UAF Polar Ionospheric Model outputs and tomography data available from the HAARP site. Finally, Chapter 6 summarizes the entire work presented and points out possible future improvements that could be achieved in the resolution of reconstructed electron densities obtained by tomography.

Chapter 2 Coordinate Systems Overview

2.1 Coordinate Systems Overview

In order to study the coordinate geometry of the GPS satellites, we need to know about two basic types of coordinate systems.

a) Cartesian Coordinate System

b) Ellipsoidal Coordinate System

Rectangular Cartesian coordinate systems represent position in space based on three perpendicular axes X, Y and Z. These three coordinate points are used to locate any point in space. An ellipsoidal coordinate system represents position in space based on two angles, latitude and longitude, and ellipsoidal height. Latitude and longitude give a position on the surface of the Earth. If the position is above the surface of the Earth, then we need to know the ellipsoidal height.

2.2 Coordinate System Transformations

In this thesis project coordinate transformations are performed to determine the GPS and Low Earth Orbit Satellites positions as well as the position of the ground station of interest. Figure 2.1 represents a point P specified in a Cartesian system (x, y) and in the associated polar coordinate system (r, Φ) in two dimensions. Figure 2.2 represents a point P specified in a Cartesian system (x, y, z) and in the associated spherical coordinate system (r, θ, Φ) in three dimensions.

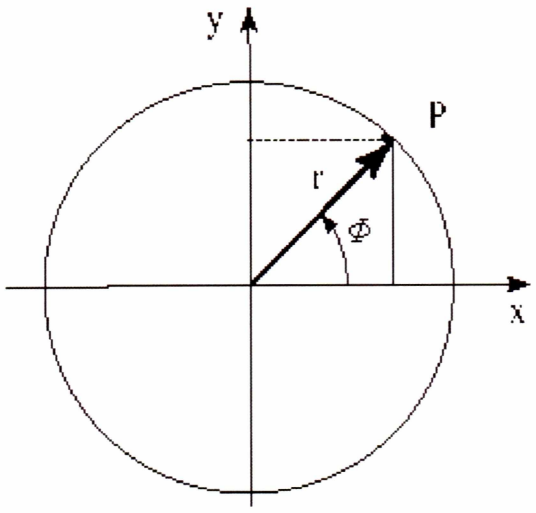

Figure 2.1 Two-dimensional coordinate system

The azimuthal angle Φ takes on values from 0 to 360 degrees and relates to longitude, and the polar angle θ takes on values from 0 to 180 degrees and relates to co-latitude.

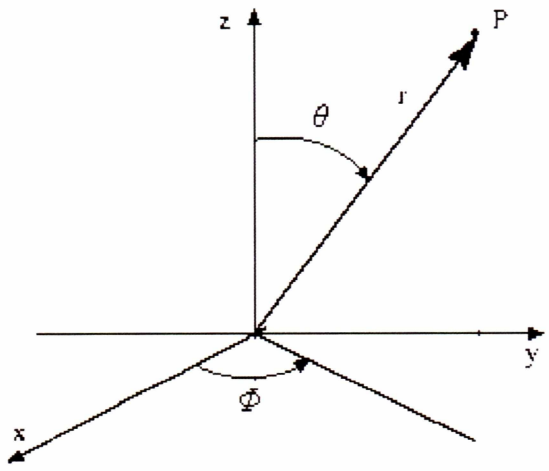

Figure 2.2 Three dimensional coordinate system

2.2.1 Ellipsoidal to Cartesian Coordinate Conversion

Ellipsoidal coordinates, in this case latitude, longitude and ellipsoidal height *(λ, θ, H),* can be converted to Cartesian coordinates *(x, y, z)* by simple mathematical equations. Values are required for the following constants: semi-major axis and semi-minor axes *a* and *b*, and ellipsoidal height *H*. The eccentricity e can be calculated from

$$e^2 = \frac{a^2 - b^2}{a^2}. \tag{2.1}$$

Transformation formulas are given by following equations

$$v = \frac{a}{\sqrt{1 - e^2 \sin^2 \phi}}, \tag{2.2}$$

$$X = (v + H)\cos\phi\cos\lambda, \tag{2.3}$$

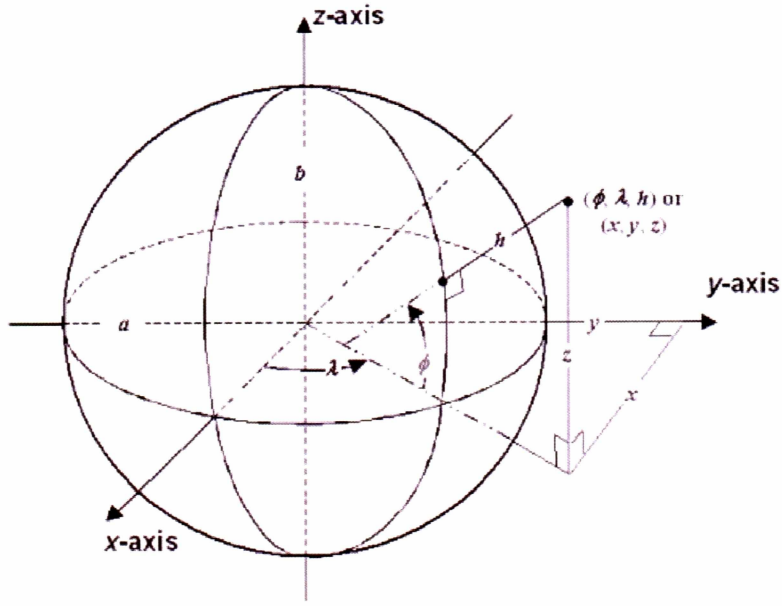

Figure 2.3 Transformation of coordinate systems [Parkinson, 1996]

$$Y = (v + H)\cos\phi \sin\lambda, \tag{2.4}$$

and

$$Z = ((1 - e^2)v + H)\sin\phi. \tag{2.5}$$

In this way latitude, longitude and ellipsoidal height are transformed into rectangular coordinates (x, y, z). Reference to these Equations is from [Parkinson, 1996] where relationship between Cartesian and Elliptical coordinates is discussed.

2.2.2 Cartesian to Ellipsoidal Coordinates Conversion

Longitude is expressed by the inverse tangent of Cartesian coordinates, given by

$$\lambda = \arctan\left(\frac{y}{x}\right). \tag{2.6}$$

Latitude is obtained by an iterative procedure; the initial value of the latitude is given by

$$\phi_0 = \arctan\left(\frac{z}{p(1 - e^2)}\right), \tag{2.7}$$

where

$$p = \sqrt{x^2 + y^2}. \tag{2.8}$$

The ellipsoidal height is given by

$$H = \frac{p}{\cos\phi} - v. \tag{2.9}$$

2.3 Azimuth Angle

For analysis of the satellite orbital geometry, it is useful to define azimuth angle. Consider a location R_0 on the spherical Earth and an arbitrary location R_S in 3-D space,

defined through their respective Cartesian coordinates as (X_0, Y_0, Z_0) and (X_S, Y_S, Z_S) respectively. For simplicity we assume here a spherical Earth model. Then the radius of the Earth R is given by the following Equation

$$R = \sqrt{X_0^2 + Y_0^2 + Z_0^2} \ . \tag{2.10}$$

We can define directions to these two locations from the center of coordinates respectively as vectors $\mathbf{R_0} = \{X_0, Y_0, Z_0\}$ and $\mathbf{R_S} = \{X_S, Y_S, Z_S\}$. Then at the location R_0 the azimuth angle to the point R_S is defined as the angle between the North direction and the direction to location R_S, both projected to the plane tangent to the sphere at the location R_0. This definition and the geometric orientations are illustrated in Figure 2.4.

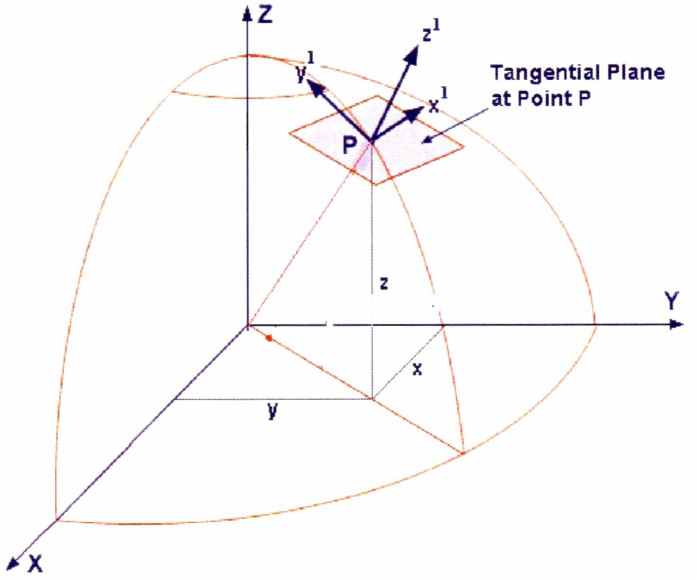

Figure 2.4 Tangential plane for azimuth angle definition, [Parkinson, 1996]

Let us consider the North Pole of Earth located at R_n with Cartesian coordinates $(X_n, Y_n, Z_n) = (0, 0, R)$. The direction to the North Pole from the coordinate center (it coincides with the Earth center) is $\mathbf{R_n} = \{X_n, Y_n, Z_n\} = \{0, 0, R\}$. At any location on the sphere R_0 we can find the azimuth angle to arbitrary location in 3-D space R_S if we introduce the tangential plane, which is orthogonal to the Earth radius at this location $\mathbf{R_0} = \{X_0, Y_0, Z_0\}$. Note that normal vector **n** in the local up-direction at the point R_0 coincides with the Earth radius-vector $\mathbf{R_0} = \{X_0, Y_0, Z_0\}$. Components of this vector are $\mathbf{n} = \{X_0, Y_0, Z_0\} = \mathbf{R_0}$. Another vector $\mathbf{X} = \{x, y, z\}$ is directed from the sphere center (0,0,0) to an arbitrary location (x, y, z) at this tangent plane such as the vector difference $\mathbf{X} - \mathbf{n} = \mathbf{p}$ comprises vector **p**, which completely belongs to the tangent plane. Equation of this tangent plane is the dot product $\mathbf{n} \bullet \mathbf{X} = R_0^2$ of these two vectors **n** and **X**. Equation (2.11) expresses the relationship between two vectors in terms of vector components

$$X_0 x + Y_0 y + Z_0 z = R_0^2 \ . \tag{2.11}$$

Note that if vectors **X** and $\mathbf{R_0}$ are completely coincide such as $\mathbf{X} = \mathbf{R_0} = \{X_0, Y_0, Z_0\}$, the Equation (2.12) yields $X_0^2 + Y_0^2 + Z_0^2 = R_0^2$, which also follows independently from equation of sphere of radius R_0.

Let us introduce an arbitrary vector $\mathbf{A} = \{A_x, A_y, A_z\}$. Projection $\mathbf{A_p}$ (2.12) of this vector **A** to the tangential plane can be represented as a difference between the initial vector **A** and its projection to the normal to this plane $\mathbf{A_n}$,

$$\mathbf{A}_p = \mathbf{A} - \mathbf{A}_n . \tag{2.12}$$

Projection $\mathbf{A}_n$ of vector $\mathbf{A}$ to the normal to the tangential plane is defined as the scalar or dot product of the unit normal vector and the initial vector $\mathbf{A}$. Since the unit normal vector for the tangential plane is given by

$$\frac{\mathbf{n}}{|\mathbf{n}|} = \frac{\{X_0, Y_0, Z_0\}}{\sqrt{R^2}} = \frac{\{X_0, Y_0, Z_0\}}{R} \tag{2.13}$$

the dot product, which defines magnitude of the projection $\mathbf{A}_n$, is

$$\mathbf{A} \bullet \frac{\mathbf{n}}{|\mathbf{n}|} = \frac{\left(A_x X_0 + A_y Y_0 + A_z Z_0\right)}{\sqrt{\left(X_0^2 + Y_0^2 + Z_0^2\right)}} \equiv S. \tag{2.14}$$

Now we can find projection $\mathbf{A}_n$ to the normal to the tangent plane using its magnitude S and unit vector $\mathbf{n}/|\mathbf{n}|$ defining local up-direction

$$\mathbf{A}_n = S\frac{\mathbf{n}}{|\mathbf{n}|} = \frac{\left(A_x X_0 + A_y Y_0 + A_z Z_0\right)}{\sqrt{\left(X_0^2 + Y_0^2 + Z_0^2\right)}} \frac{\{X_0,\ Y_0,\ Z_0\}}{\sqrt{\left(X_0^2 + Y_0^2 + Z_0^2\right)}} \equiv C\{X_0,\ Y_0,\ Z_0\}, \tag{2.15}$$

where $$C = \frac{\left(A_x X_0 + A_y Y_0 + A_z Z_0\right)}{X_0^2 + Y_0^2 + Z_0^2} = \frac{\left(A_x X_0 + A_y Y_0 + A_z Z_0\right)}{R^2} . \tag{2.16}$$

From Equation 2.13, projection $\mathbf{A_p}$ to the tangential plane is the vector difference between the initial vector $\mathbf{A}$ and its projection $\mathbf{A_n}$ to the normal to this plane

$$\mathbf{A_p} = \mathbf{A} - \mathbf{A_n} = \{A_x - CX_0, A_y - CY_0, A_z - CZ_0\}, \tag{2.17}$$

where parameter C is defined in (2.16).

Having derived equations above for arbitrary vector, now we can apply these expressions for vectors of our interest merely by substituting the vector components. The location of our interest at (X_0, Y_0, Z_0) is also defined by vector $\mathbf{R_0}=\{X_0, Y_0, Z_0\}$, originating at the coordinate center. The direction from this location to the North Pole at (X_n, Y_n, Z_n) = (0, 0, R) (which is defined also by vector $\mathbf{R_n}$ = {0, 0, R}), can be found as a difference of the corresponding vectors

$$\mathbf{R_{n0}} = \mathbf{R_n} - \mathbf{R_0} = \{X_n - X_o, Y_n - Y_o, Z_n - Z_o\} = \{-X_o, -Y_o, R - Z_o\}. \tag{2.18}$$

Applying Equations (1.16-1.18), now we can find projection of vector $\mathbf{R_{no}}$ from (2.18) to the tangential plane

$$\mathbf{R^p_{n0}} = \mathbf{R_{n0}} - \mathbf{R^n_{n0}} = \{-X_0 - C_{n0}X_0, \; -Y_0 - C_{n0}Y_0, \; R - Z_0 - C_{n0}Z_0\} =$$
$$\{-X_0(1+C_{n0}), \; -Y_0(1+C_{n0}), \; R - Z_0(1+C_{n0})\} = \left\{-X_0\frac{Z_0}{R}, \; -Y_0\frac{Z_0}{R}, \; R - Z_0\frac{Z_0}{R}\right\}, \tag{2.19}$$

Where $C_{n0} = -\frac{X_0^2}{R^2} - \frac{Y_0^2}{R^2} + (R - Z_0)\frac{Z_0}{R^2} = \frac{Z_0}{R} - 1$.

To complete determination of the azimuth angle, we need to define projection on the tangential plane for the second vector in the direction from the ground location R_0 to an arbitrary point in 3-D space R_S. This direction (Equation 2.20) and its projection to the plane (Equation 2.22) can be defined as follows

$$\mathbf{R_{S0}} = \mathbf{R_S} - \mathbf{R_0} = \{X_S - X_0,\ Y_S - Y_0,\ Z_S - Z_0\} \tag{2.20}$$

$$\begin{aligned} &\mathbf{R}^{\mathbf{p}}_{\mathbf{S0}} = \mathbf{R_{S0}} - \mathbf{R}^{\mathbf{n}}_{\mathbf{S0}} = \\ &\{X_S - X_0 - C_{S0}X_0, Y_S - Y_0 - C_{S0}Y_0, Z_S - Z_0 - C_{S0}Z_0\} = \\ &\{X_S - X_0(1 + C_{S0}), Y_S - Y_0(1 + C_{S0}), Z_S - Z_0(1 + C_{S0})\} = \\ &\{X_S - X_0 C^1_{S0}, Y_S - Y_0 C^1_{S0}, Z_S - Z_0 C^1_{S0}\}, \end{aligned} \tag{2.21}$$

where parameters C_{S0} and C^1_{S0} are introduced for convenience

$$C_{S0} = \left[(X_s - X_0)X_0 - (Y_s - Y_0)Y_0 + (Z_s - Z_0)\right]\frac{Z_0}{R^2} = \frac{\left[X_S X_0 + Y_S Y_0 + Y_S Y_0\right]}{R^2} - 1 \equiv C^1_{S0} - 1. \tag{2.22}$$

The azimuth angle α was defined above as an angle between projections of the vectors $\mathbf{R_{n0}}$ and $\mathbf{R_{S0}}$ to the tangential plane. We denote these projection vectors as $\mathbf{R}^{\mathbf{p}}_{\mathbf{n0}}$ and $\mathbf{R}^{\mathbf{p}}_{\mathbf{S0}}$ respectively. To find this angle, it is necessary to take the scalar or dot product of the projections above with explicit substitution of their coordinates, which has been determined earlier in Equations (2.19) and (2.21)

$$\alpha = Cos^{-1}\frac{\left(\mathbf{R}^{\mathbf{p}}_{\mathbf{n0}} \bullet \mathbf{R}^{\mathbf{p}}_{\mathbf{S0}}\right)}{\left|\mathbf{R}^{\mathbf{p}}_{\mathbf{n0}}\right|\left|\mathbf{R}^{\mathbf{p}}_{\mathbf{S0}}\right|} =$$

(2.23)

$$= Cos^{-1}\left[\frac{\left\{-X_0 Z_0 \frac{(X_S - X_0 C^1_{S0})}{R} - Y_0 Z_0 \frac{(Y_S - Y_0 C^1_{S0})}{R} + (R - Z_0 \frac{Z_0}{R})(Z_S - Z_0 C^1_{S0}\right\}}{\left(\sqrt{\left(X_0 \frac{Z_0}{R}\right)^2 + \left(Y_0 \frac{Z_0}{R}\right)^2 + \left(R - Z_0 \frac{Z_0}{R}\right)^2}\right)\left(\sqrt{\left(X_S - X_0 C^1_{S0}\right)^2 + \left(Y_S - Y_0 C^1_{S0}\right)^2 + \left(Z_S - Z_0 C^1_{S0}\right)^2}\right)}\right].$$

Equation (2.23) generally defines the azimuth angle to an arbitrary location R_s in 3-D space at the point R_0 on the surface of the Earth through the Cartesian coordinates of the relevant locations. However, this expression (2.23) defines azimuth angle in the interval $[0,\pi]$ as the main value of *arcos*-function. It is still necessary to distinguish between cases of clockwise and anti-clockwise orientation of $\mathbf{R}^{\mathbf{p}}_{\mathbf{S0}}$ with respect to $\mathbf{R}^{\mathbf{p}}_{\mathbf{n0}}$. If former is true, a correction of azimuth angle from (2.23) to $2\pi - \alpha$ needs to be applied.

To find out the difference in the vectors' orientation, we will take the cross product of two projections above and compare the direction of the resulting cross product with the local up-direction. If these up-direction and cross-product vectors are anti-parallel, it indicates anti-clockwise orientation of $\mathbf{R}^{\mathbf{p}}_{\mathbf{S0}}$ with respect to $\mathbf{R}^{\mathbf{p}}_{\mathbf{n0}}$ and a need for correction of $2\pi - \alpha$ for the final expression of the azimuth angle. Anti-parallelism of two vectors takes place if their dot product is negative. Hence, a condition for the azimuth angle correction is expressed in (2.24) and in (2.25).

$$\frac{\mathbf{n}}{|\mathbf{n}|}\bullet\left[\mathbf{R}^{\mathbf{p}}_{\mathbf{S0}}\times\mathbf{R}^{\mathbf{p}}_{\mathbf{n0}}\right]<0 \quad\Rightarrow\quad \alpha=2\pi-Cos^{-1}\frac{\left(\mathbf{R}^{\mathbf{p}}_{\mathbf{n0}}\bullet\mathbf{R}^{\mathbf{p}}_{\mathbf{S0}}\right)}{\left|\mathbf{R}^{\mathbf{p}}_{\mathbf{n0}}\right|\left|\mathbf{R}^{\mathbf{p}}_{\mathbf{S0}}\right|} \tag{2.24}$$

$$\frac{\mathbf{n}}{|\mathbf{n}|}\bullet\left[\mathbf{R}^{\mathbf{p}}_{\mathbf{S0}}\times\mathbf{R}^{\mathbf{p}}_{\mathbf{n0}}\right]>0 \quad\Rightarrow\quad \alpha=Cos^{-1}\frac{\left(\mathbf{R}^{\mathbf{p}}_{\mathbf{n0}}\bullet\mathbf{R}^{\mathbf{p}}_{\mathbf{S0}}\right)}{\left|\mathbf{R}^{\mathbf{p}}_{\mathbf{n0}}\right|\left|\mathbf{R}^{\mathbf{p}}_{\mathbf{S0}}\right|} \tag{2.25}$$

The expression for cross product of the projections is

$$\mathbf{R}^{\mathbf{p}}_{\mathbf{S0}}\times\mathbf{R}^{\mathbf{p}}_{\mathbf{n0}} = \begin{vmatrix} \hat{\mathbf{i}} & \hat{\mathbf{j}} & \hat{\mathbf{k}} \\ X_S-X_0(1+C_{S0}) & Y_S-Y_0(1+C_{S0}) & Z_S-Z_0(1+C_{S0}) \\ -X_0\dfrac{Z_0}{R} & -Y_0\dfrac{Z_0}{R} & R-Z_0\dfrac{Z_0}{R} \end{vmatrix} =$$

$$\begin{aligned}
&= \hat{\mathbf{i}}\left[\left(Y_S-Y_0(1+C_{S0})\right)\left(R-Z_0\frac{Z_0}{R}\right)-\left(Z_S-Z_0(1+C_{S0})\right)\left(-Y_0\frac{Z_0}{R}\right)\right] \\
&\quad+\hat{\mathbf{j}}\left[\left(-X_0\frac{Z_0}{R}\right)\left(Z_S-Z_0(1+C_{S0})\right)-\left(R-Z_0\frac{Z_0}{R}\right)\left(X_S-X_0(1+C_{S0})\right)\right] \\
&\quad+\hat{\mathbf{k}}\left[\left(X_S-X_0(1+C_{S0})\right)\left(-Y_0\frac{Z_0}{R}\right)-\left(Y_S-Y_0(1+C_{S0})\right)\left(-X_0\frac{Z_0}{R}\right)\right] \\
&= \hat{\mathbf{i}}\left[\left(Y_S-Y_0C^1_{S0}\right)\left(R-Z_0\frac{Z_0}{R}\right)-\left(Z_S-Z_0C^1_{S0}\right)\left(-Y_0\frac{Z_0}{R}\right)\right] \\
&\quad+\hat{\mathbf{j}}\left[\left(-X_0\frac{Z_0}{R}\right)\left(Z_S-Z_0C^1_{S0}\right)-\left(R-Z_0\frac{Z_0}{R}\right)\left(X_S-X_0C^1_{S0}\right)\right] \\
&\quad+\hat{\mathbf{k}}\left[\left(X_S-X_0C^1_{S0}\right)\left(-Y_0\frac{Z_0}{R}\right)-\left(Y_S-Y_0C^1_{S0}\right)\left(-X_0\frac{Z_0}{R}\right)\right]
\end{aligned} \tag{2.26}$$

where $1+C_{S0}=C^1_{S0}$. Now, the dot product of vector $\mathbf{R}^{\mathbf{p}}_{\mathbf{s0}}\times\mathbf{R}^{\mathbf{p}}_{\mathbf{n0}}$ and the unit up-vector $\frac{\mathbf{n}}{|\mathbf{n}|}$ is given by the expression in Equation 2.27.

$$\frac{\mathbf{n}}{|\mathbf{n}|}\bullet\left[\mathbf{R}_{S0}^{p}\times\mathbf{R}_{n0}^{p}\right]=\frac{1}{\sqrt{R^2}}\left\{\begin{array}{l}\hat{\mathbf{i}}\left[\left(Y_S-Y_0(1+C_{S0})\right)\left(R-Z_0\frac{Z_0}{R}\right)-\left(Z_S-Z_0(1+C_{S0})\right)\left(-Y_0\frac{Z_0}{R}\right)\right]\\+\hat{\mathbf{j}}\left[\left(-X_0\frac{Z_0}{R}\right)\left(Z_S-Z_0(1+C_{S0})\right)-\left(R-Z_0\frac{Z_0}{R}\right)\left(X_S-X_0(1+C_{S0})\right)\right]\\+\hat{\mathbf{k}}\left[\left(X_S-X_0(1+C_{S0})\right)\left(-Y_0\frac{Z_0}{R}\right)-\left(Y_S-Y_0(1+C_{S0})\right)\left(-X_0\frac{Z_0}{R}\right)\right]\end{array}\right\} \tag{2.27}$$

$$=\frac{1}{\sqrt{R^2}}\left\{\begin{array}{l}\hat{\mathbf{i}}\left[\left(Y_S-Y_0C_{S0}^{1}\right)\left(R-Z_0\frac{Z_0}{R}\right)-\left(Z_S-Z_0C_{S0}^{1}\right)\left(-Y_0\frac{Z_0}{R}\right)\right]\\+\hat{\mathbf{j}}\left[\left(-X_0\frac{Z_0}{R}\right)\left(Z_S-Z_0C_{s0}^{1}\right)-\left(R-Z_0\frac{Z_0}{R}\right)\left(X_S-X_0C_{S0}^{1}\right)\right]\\+\hat{\mathbf{k}}\left[\left(X_S-X_0C_{S0}^{1}\right)\left(-Y_0\frac{Z_0}{R}\right)-\left(Y_S-Y_0C_{S0}^{1}\right)\left(-X_0\frac{Z_0}{R}\right)\right]\end{array}\right\}$$

using definition $1+C_{S0}=C_{S0}^{1}$. A positive or negative value of expression (2.27) finally defines azimuth angle α according to Equations (2.25) and/or (2. 26) respectively.

2.4 Elevation Angle

The elevation angle of an object is defined as the angle between the horizontal and the line of sight to the object (Figure 2.5).

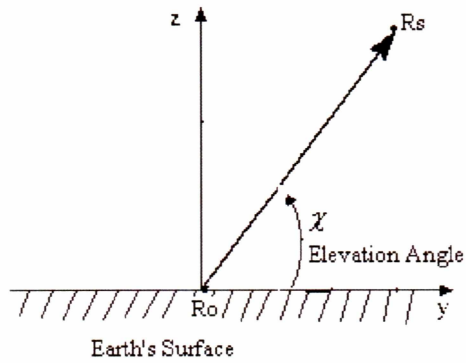

Figure 2.5 Elevation angle between satellite and ground plane

Let us consider two locations, a ground location on the surface of the Earth R_0 with Cartesian coordinates (X_0, Y_0, Z_0) and a satellite in space at an arbitrary point R_S with coordinates (X_S, Y_S, Z_S). For convenience, the surface location R_0 can also be represented through its latitude ϕ and longitude λ. Elevation angle defined as above is the angle supplemental to the angle between local up-direction and the direction to the satellite. Therefore, the cosine of this supplemental angle can be determined by the dot product of unit vectors along these two directions. If we define $\hat{\mathbf{i}}$, $\hat{\mathbf{j}}$, $\hat{\mathbf{k}}$ as the unit vectors in the directions of X-, Y-, and Z-axis of the Cartesian frame respectively, then the local up-direction is $\hat{\mathbf{i}}\, Cos\phi\, Cos\lambda + \hat{\mathbf{j}}\, Cos\phi\, Sin\lambda + \hat{\mathbf{k}}\, Sin\phi$. Direction from the ground location R_0 to an arbitrary location in 3-D space R_S can be expressed as $\hat{\mathbf{i}}\,(X_S - X_0) + \hat{\mathbf{j}}\,(Y_S - Y_0) + \hat{\mathbf{k}}\,(Z_S - Z_0)$ in the Cartesian frame. Upon normalization, the unit vector $\mathbf{R_S}/|\mathbf{R_S}|$ in this direction $\mathbf{R_S}$ is

$$\frac{\mathbf{R_S}}{|\mathbf{R_S}|} = \frac{\hat{\mathbf{i}}\,(X_S - X_0) + \hat{\mathbf{j}}\,(Y_S - Y_0) + \hat{\mathbf{k}}\,(Z_S - Z_0)}{\sqrt{(X_S - X_0)^2 + (Y_S - Y_0)^2 + (Z_S - Z_0)^2}}. \tag{2.28}$$

The angle between local up-direction $\mathbf{R_0}$ and direction $\mathbf{R_S}$ to the object with coordinates (X_S, Y_S, Z_S) can be determined from the dot product of two vectors defining these directions as soon as the components of these vectors are known. The components of the unit vector in the local up-direction $\mathbf{R_0}$ in terms of the geographic coordinates of the location of interest and components of unit vector in direction $\mathbf{R_S}$ are, respectively

$$\frac{\mathbf{R_0}}{|\mathbf{R_0}|} = \{\ Cos\phi\, Cos\lambda,\ Cos\phi\, Sin\lambda,\ Sin\phi\ \} \tag{2.29}$$

$$\frac{\mathbf{R_S}}{|\mathbf{R_S}|} = \left\{ \begin{array}{c} \dfrac{(X_S - X_0)}{\sqrt{(X_S - X_0)^2 + (Y_S - Y_0)^2 + (Z_S - Z_0)^2}}, \\ \dfrac{(Y_S - Y_0)}{\sqrt{(X_S - X_0)^2 + (Y_S - Y_0)^2 + (Z_S - Z_0)^2}}, \\ \dfrac{(Z_S - Z_0)}{\sqrt{(X_S - X_0)^2 + (Y_S - Y_0)^2 + (Z_S - Z_0)^2}} \end{array} \right\}. \tag{2.30}$$

Substituting these components into the standard dot-product expression for two unit vectors $\mathbf{a} \bullet \mathbf{b} = Cos(\mathbf{a}, \mathbf{b}) = a_x b_x + a_y b_y + a_z b_z$, we can determine elevation angle χ using

$$Cos\left(\frac{\pi}{2} - \chi\right) = Sin\chi = \left\{ \frac{(X_S - X_0)Cos\phi\, Cos\lambda + (Y_S - Y_0)Cos\phi\, Sin\lambda + (Z_S - Z_0)Sin\phi}{\sqrt{(X_S - X_0)^2 + (Y_S - Y_0)^2 + (Z_S - Z_0)^2}} \right\} \tag{2.31a}$$

and, finally,

$$\chi = Sin^{-1}\left\{ \frac{(X_S - X_0)Cos\phi\, Cos\lambda + (Y_S - Y_0)Cos\phi\, Sin\lambda + (Z_S - Z_0)Sin\phi}{\sqrt{(X_S - X_0)^2 + (Y_S - Y_0)^2 + (Z_S - Z_0)^2}} \right\} \tag{2.31}$$

2.5 Determination of 3-D Angle between Magnetic field and Propagation

Let's define a coordinate system East-North-Up (**ExN=U**), with its origin at a ground location on the Earth's surface. The unit vector in the direction of the magnetic field is defined by the dip (inclination) and declination angles. Direction of dip angle *I* of the magnetic field with respect to the horizontal plane at a given geographic point is

assumed positive in the Northern Hemisphere, where the magnetic field is oriented downward. Thus a dip angle of 90 degrees corresponds to the vertical orientation of the magnetic field. The declination angle D is defined as an angle between the horizontal direction of the magnetic field and local north. Eastward direction is assumed positive [Maurits, 1996]. Than we can define the components of the unit vector of direction of the magnetic field (MF) as

$$\mathbf{U}^{MF} = \left\{ U_x^{MF},\ U_y^{MF},\ U_z^{MF} \right\} = \{ Cos\, I\, Sin\, D,\ \ Cos\, I\, Cos\, D,\ \ -Sin\, I \}. \qquad (2.32)$$

Parameters for angular representation of the magnetic field components are available for any geographic location from various magnetic filed models, adjustable to the current epoch.

The unit vector in the direction from receiver to satellite is defined by the satellite elevation angle χ and azimuth angle α. The Elevation angle χ is the angle between line of sight to the satellite and the horizontal plane at a given geographic point. It is defined positive if the satellite is above the local horizon. For reference, elevation angle equal to 90 degrees or $\pi/2$ corresponds to the signal vertical propagation. Azimuth angle α is the angle between local North and projection of the signal propagation direction on the plane tangential to the Earth at the origin of our coordinate systems. The eastward direction of azimuth angle is assumed positive. Using such definitions, components of the unit vector in the direction from receiver to the satellite can be expressed as follows

(we denote this direction as -SP to indicate that it is a direction opposite to direction of the actual signal propagation SP),

$$\mathbf{U}^{-SP} = \left\{ U_x^{-SP},\ U_y^{-SP},\ U_z^{-SP} \right\} = \{Cos\chi\, Sin\alpha,\ Cos\chi\, Cos\alpha,\ Sin\chi\}. \tag{2.33}$$

Correspondingly, the unit vector in the opposite direction, from satellite to the receiver (direction of actual signal propagation) is $-\mathbf{U}^{-SP} = \mathbf{U}^{SP}$ and

$$\begin{aligned} \mathbf{U}^{SP} &= \left\{ -U_x^{-SP}, -U_y^{-SP}, -U_z^{-SP} \right\} = \left\{ U_x^{SP},\ U_y^{SP},\ U_z^{SP} \right\} = \\ &= \{ -Cos\chi\, Sin\alpha,\ -Cos\chi\, Cos\alpha,\ -Sin\chi \} = \left\{ Cos\chi\, Sin\alpha^1,\ Cos\chi\, Cos\alpha^1,\ -Sin\chi \right\} \end{aligned} \tag{2.34}$$

where the definition of $\alpha^1 = \alpha + \pi$ indicates that the azimuth angle α of direction to the satellite is opposite to the azimuth angle of direction from the satellite α^1.

Taking the dot product of two vectors defined in (2.33) and (2.35), we can derive the expression for angle between the magnetic field and the signal propagation direction β as follows.

$$\begin{aligned} \beta &= Cos^{-1}\left[U_x^{MF} U_x^{SP} + U_y^{MF} U_y^{SP} + U_z^{MF} U_z^{SP}) \right] = \\ &= Cos^{-1}\left[CosI\, SinD\, Cos\chi\, Sin\alpha + CosI\, SinD\, Cos\chi\ \ Sin\alpha + SinI\, Sin\chi \right] \end{aligned} \tag{2.35}$$

It is instructive to consider important special cases using expression (2.35). For orientations of the satellite when dip angle is equal to the elevation angle, $I = \chi$, and declination angle is equal to the azimuth angle, $D = \alpha$, it means that the magnetic field and signal propagation direction are in the same plane, but their azimuths differ by 180 degrees or π. In this case the angle between the magnetic field and signal propagation direction is defined by the elevation angle such as

$$\beta(\chi = I,\ \alpha = D) = Cos^{-1}\left(Sin^2 I - Cos^2 I\right) = Cos^{-1}\left(Sin^2 \chi - Cos^2 \chi\right) = \tag{2.36a}$$

$$= Cos^{-1}\left(-Cos\ 2\chi\right) = Cos^{-1}\left(Cos\ (\pi - 2\chi)\right) = \pi - 2\chi = \pi - 2I,$$

which can be shown alternatively just from consideration of the geometry of this case. If $D = \alpha + 180 = \alpha^1$ and $I = \chi$, this case means that the magnetic field and the signal propagation direction are parallel and, hence, angle β between them is zero. Indeed, substitution to (2.35) yields

$$\beta(\chi = I,\ D = a + \pi) = Cos^{-1}\left(Sin^2 I + Cos^2 I\right) = Cos^{-1}\left(Sin^2 \chi + Cos^2 \chi\right) = 0. \tag{2.36b}$$

The equation 2.35 above defines the angle between the magnetic field, expressed through its angular components, and the signal propagation direction through χ and α (elevation angle and azimuth angle of direction to the satellite). These angles were derived in previous sections of this chapter in terms of known geographic coordinates of

the location of interest on the Earth surface and the Cartesian coordinates of the satellite. This representation of the satellite coordinates in Cartesian frame is standard in satellite navigation. For each NORAD-cataloged satellite, its Cartesian coordinates are available for each time instant either through computations using the satellite orbital elements, or, optionally, from the real-time tracking systems of important satellites such as GPS constellation.

Thus, expressions derived above completely define the geometric description of the satellite-receiver mutual location and its orientation with respect to the Earth magnetic field through readily available elements and parameters.

2.6 Modern GPS Coordinate Systems

2.6.1 The International GPS Service (IGS)

International GPS Service (IGS) operates 296 GPS stations all around the world and produces various kinds of products like dual-frequency GPS data, precise GPS satellite orbits, clock parameters, tracking station coordinates and velocities. These products are available on-line. Dual-frequency GPS data are used for fine-precision position calculations [Beutler, 1995].

2.6.2 SP3 Format

SP3 (Standard Product # 3) is one standard orbit format for GPS satellites. The basic format is a position and clock record; a second, optional, record contains velocities

and clock rates-of-change. There are 24 lines in this format and each line has different columns. Each column holds information about a particular satellite location, velocity, GPS precise time format, etc. The SP3 format has been designed such that satellites other than GPS could be described as well.

In this thesis project, we read the real-time updated GPS satellite coordinates from SP3 data. Initially we download the current SP3 files from an on-line server, using a UNIX utility *lynx* and store them locally. FORTRAN code then reads the satellite's coordinates *(X, Y, Z)* and GPS time from the SP3 data and these values are used for the emulation of other parameters. This process is more elaborately described in Chapter 4 of this thesis.

Chapter 3 The Ionosphere and its Monitoring

3.1 The Ionosphere and its Structure

The ionosphere begins at approximately 60 km from the surface of the Earth and extends to around 1000 km. It is basically formed by ionization of molecules due to solar radiation (UV, X radiation). Maximum ionization typically occurs in the range of 200 to 400 km height. The overall charge of the ionosphere is zero, i.e., equal numbers of electrons and positive ions. The ionosphere is generally divided in to several layers based on their ionization process. Figure 3.1 shows the various levels of the ionosphere.

- **D layer** is the lowest layer, found between 60 to 90 km from the surface of the Earth, is normally generated by the hard X-radiation of the sun.
- **E layer**, from 90 km to 130 km, is generated by soft X-radiation. This layer is present predominantly in daytime and decreases at night.
- **F layer** is the predominant layer in an electron density profile and contains the highest electron densities. This layer is sub-divided in two:
    - **Fl layer**, from 130 km to 210 km, which is present only during daytime and can be distinguished as an inflexion in the profile.
    - **F2 layer**, from 210 km to l000 km, which contains the maximum of the electron density profile.

Layers are divided based on their electron density along the density profile. Each layer is distinguishable by differences in physical processes like absorption and recombination.

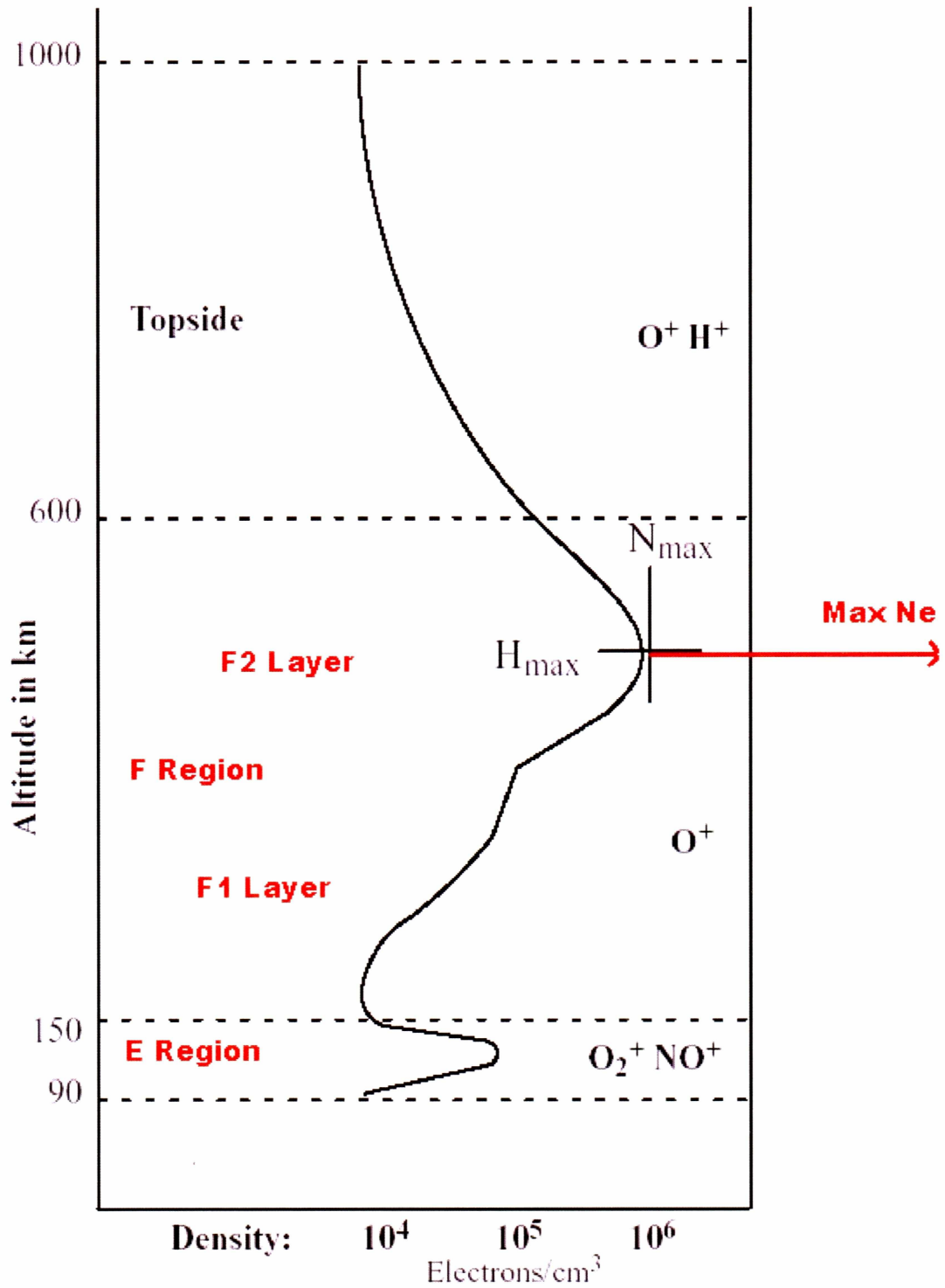

Figure 3.1 Electron-density (Ne) profile along the ionosphere, [Al'Pert, 1974]

They are also distinguishable based on the level of ionization. Table 3.1 shows each layer and its typical range of electron density values. As can be seen in Table 3.1, the D and F1 regions vanish at night and the E region becomes very weak. The F2 region diminishes continuously but still possesses a considerable electron density by sunrise, when the ionization process starts again.

Table 3.1 Ionospheric layers and their electron content

Region	**Altitude (km)**	**N_e peak (cm^{-3})**
D	90	$1.5e10^4$ Day 0 Night
E	120	$1.5e10^5$ Day $<1e10^3$ Night
F1	200	$2.5e10^5$ Day $1e10^5$ Night
F2	300	10^6 Day 10^4 Night

3.2 Modeling of the Ionosphere

Ionospheric models are basically classified into three categories:

1) Theoretical Models

2) Empirical Models

3) Statistical Models

Theoretical models are very complex and require high-speed computers. These models provide ionospheric information as a function of height, location, and time through the application of equations that describe the physical and chemical processes present in the ionosphere. For statistical models, ionospheric parameters are determined based on data observed throughout the world.

The third class of models, empirical models, combines both of the other model types. The theoretical models are used for the lower ionosphere while the statistical models are used for the upper ionosphere.

A model is used to duplicate and thus predict the ionosphere, and simulations of radio wave propagation are performed to obtain ionospheric parameters like Total Electron Content, or Scintillation Parameters. Prediction can be long-term or short-term. Long-term prediction provides HF propagation parameters at any location on the Earth for a 24 hour period. These models are demonstrated in Wang, [2002].

3.3 Ionospheric Models

Ionospheric Models are used to study the changes in ionosphere and also predict the average ionospheric profile. A few examples of ionospheric models are the International Reference Ionosphere and Parameterized Ionospheric Model (PIM).

3.3.1 International Reference Ionosphere (IRI)

The IRI ionosphere model is an international standard for the specification of ionospheric densities and temperatures, which was developed by the International Union of Radio Science and the Committee on Space Research. IRI is an empirical model based on previous data records. The IRI model is being updated with measured parameters, such as the Total Electron Content emulated from GPS. It is the user's responsibility to specify the input parameters such as location and times to do these updates. Then from the updates, the corresponding IRI index is adjusted until the predicted data matches the measured data. Thus the IRI model provides a way to globally map the ionosphere.

3.4.2 Parameterized Ionospheric Model (PIM)

The Parameterized Ionospheric Model (PIM) is a theoretical ionosphere model used for real time ionosphere specification for the Air Force Air Weather Service at the Air Force Space Forecast Center. The PIM model was initially a computationally efficient model to aid development of a global Parameterized Real-time Ionospheric Specification Model [Daniell et al., 1995].

3.4 Validation of the Ionospheric Model

The main objective of this thesis is to develop tools for validation of the UAF Eulerian parallel polar ionosphere model. In this process two methods have been developed. They are:

- GPS TEC calculation method discussed in Chapter 4 of this thesis.

- Computerized Ionosphere Tomography discussed in Chapter 5 of this thesis.

Chapter 4 and 5 basically describe the basic software techniques we developed to estimate TEC and Ionospheric tomography.

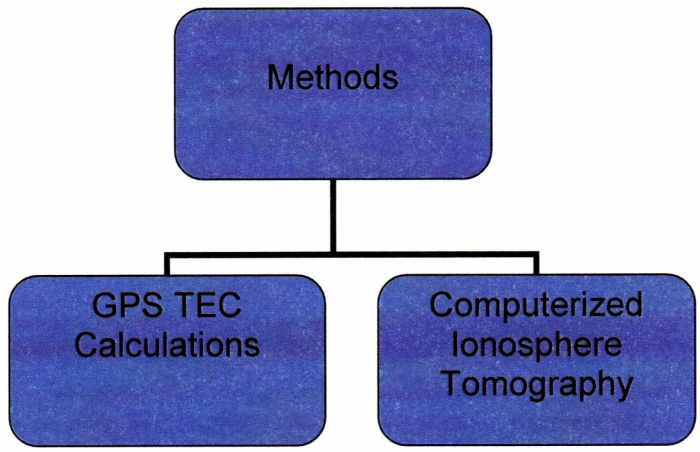

Figure 3.2 Tools for validation of the model

3.5 Propagation of a Radio Wave through the Ionosphere

When a RF wave propagates through the ionosphere, the frequency of the propagating wave changes due to irregularities in the ionosphere. The wave may be absorbed or the direction of its propagation [Hargreaves, 1992] may also be altered. In other words, the phase of the propagating wave changes as it propagates. The refractive index of the ionosphere and the phase velocity of the propagating radio wave depend on the electron density and therefore typically vary with altitude. The phase velocity

increases with an increase in the electron density and the refractive index decreases with an increase in electron density. Consider a radio wave of a particular frequency that enters the ionosphere. At first, the wave travels along the normal with the speed of light in vacuum as the density is low. But as the density increases, the phase velocity increases, the refractive index decreases and the path of the wave bends away from the normal. At this point, the wave will not propagate further into the medium but it will be reflected back towards the same side of the ionosphere from where it originated. The highest frequency of a radio wave that is reflected by a layer of electron density is called the critical frequency of that layer. A wave traveling with any frequency greater than the critical frequency will pass through the ionosphere.

3.5.1 Effect of the Ionosphere on Radio Systems

The ionosphere is used to reflect radio waves from the transmitter to the receiver, and so the maximum frequency (maximum usable frequency or MUF) that will be reflected by the ionosphere will have to be determined. Once the MUF is determined, optimum transmission frequencies can be selected for different regions and the spectrum can be shared.

Ionospheric variations affect HF circuits by focusing or de-focusing the radio signal, causing fading, and allowing propagation over two or more paths resulting in interference. Satellite communication is also affected by ionospheric disturbances. The satellite systems require a certain signal-to-noise ratio to operate normally. Ionospheric

disturbances, primarily scintillation or rapid fading, affect the propagating signal and the system will have to increase the transmitted power to maintain the same signal-to-noise ratio, thereby increasing the cost. This effect decreases with increasing frequency. Still there is some effect in the gigahertz range of frequencies that most new satellites operate in, especially in the equatorial zones and in times of high solar activity. Ground-based navigational aids use the lower ionosphere for propagation to determine the position of objects at a few hundreds of kilometers. Many of these systems use VLF (3-30 kHz) and the D region of the ionosphere, which is more stable compared to the E region. However, day-night variations exist, causing time delays over the propagation path. These delays will have to be considered in position determination. Satellite-based navigation aids overcome this problem by using higher frequencies.

The Global Positioning System (GPS) uses the frequencies 1.2 GHz and 1.6 GHz; hence even large variations in electron content will cause position errors that are small. Errors due to the ionosphere in the position measurements using single frequency receivers are about 10m. These are small enough for most applications, but for more exacting applications, like surveying, dual frequency measurements and ionospheric corrections are necessary. The older systems that are still in use, like the Navy Navigation Satellite System (NNSS), use lower frequencies. NNSS uses 150 MHz and 400 MHz signals. These are affected more by the ionosphere and position measurements have large errors due to ionospheric variations, which in principle can be eliminated using a correction with two frequencies.

3.6 Slant Total Electron Content

Slant Total Electron Content (STEC) is defined as the integral of the electron density along the signal path and is given by

$$STEC = \int_{Tx}^{Rx} N_e ds_o , \tag{3.1}$$

where STEC is measured as electrons/ m^2, where one TECU is defined as 10^{16} electrons contained in a cylinder of cross section of 1 m^2 aligned with the ray path. If the STEC is in the vertical direction, one will have Vertical TEC (VTEC, or simply TEC) instead of STEC.HAARP provides access to STEC and VTEC data. These data are published in their website and updated every hour.

3.7 Ionospheric Data

3.7.1 Ionosonde

Ionosonde is used to obtain an accurate description of total electron density distribution in the ionosphere. Fernandez, [2004] explained the importance of Ionosonde. This instrument relies on the fact that signals traveling at particular frequency (under 20 MHz) are reflected back by the different layers of the ionosphere.

The operation of this instrument consists in the emission and reception of signals from 0.1 MHz to 30 MHz in the vertical direction. For each frequency the travel time of the signal to go upwards and downwards again, due to the reflection of the different ionospheric layers, is measured. The electron density present in the ionosphere defines

the maximum frequency for which the signals are no longer reflected. This relationship is stated through the following expression

$$f_c^2 = \frac{e^2}{4\pi^2 \varepsilon_o m_e} N_{\max}, \tag{3.2}$$

where e is the charge of the electron, m_e the mass of an electron and ε_o the permittivity of free space. The peak value of the electron density (N_{max}) is expressed in electrons per cubic meter and the corresponding critical frequency (f_c) is in units of Hertz. If the signal has a larger frequency than the critical frequency of the layer (f_c), it will not reflect the signal and therefore it will continue to propagate upwards. When the critical frequency of the F2 layer is reached (corresponding to the maximum of electron density or NmF2), signals with greater frequency will not be reflected anymore and will travel to space.

With the travel time it is possible to obtain the apparent height of the ionized layer *(virtual height),* defined as

$$h' = \frac{c\tau}{2}, \tag{3.3}$$

where τ is the travel time and c is the speed of light. This height is not real but virtual since the pulse is delayed by the ionized layers, and instrumental delays. The plots of virtual height against frequency are called *ionograms*.

3.7.2 Conversion of Real-time HAARP Ionosonde Data Files

Real-time Ionosonde text files are used for plotting critical frequency (foF2) values, which is defined as the frequency at which RF wave propagation delay varies in accordance to density of electrons. Numerical emulation of the critical frequency (foF2, [MHz]) measurements is performed during the UAF EPPIM forecasting real-time run. The measured foF2 from the text file and the calculated foF2 from the model are the compared in this thesis project. The sample text file is shown in the Appendix of this thesis. Figure 3.3 obtained from our website http://www.arsc.edu/SpaceWeather/ shows UAF EPPIM forecasted foF2's in black curves and the red triangles indicate the measured foF2's, in this case obtained from the text file.

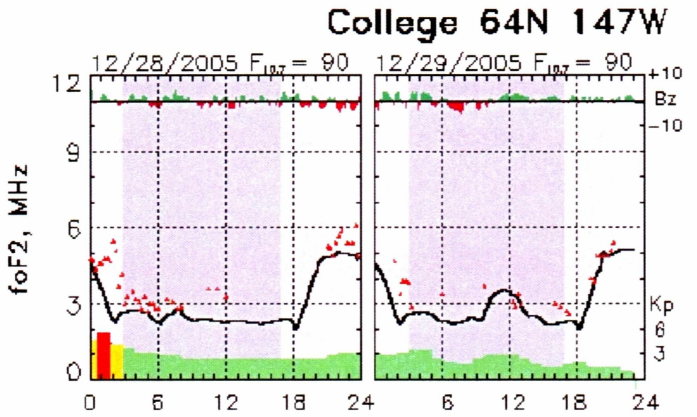

Figure 3.3 Real-time foF2 comparisons

3.7.2.1 Standard Archiving Output (SAO) Format

The SAO format was originally designed for storing Digisonde ionograms scaled by the auto scaling software ARTIST and edited using the ADEP utility. However, in

subsequent releases a special effort was made to generalize SAO design so that it can hold scaled data produced by other sounder systems. With the release of version 4.1, the degree of format universality became high enough to promote SAO as a standard format for exchange of scaled ionogram data.

3.7.2.2 Fetching and Reading of SAO Files

The SAO files are obtained in real-time for the HAARP site at Gakona in a web-accessible database. Files are fetched using lynx utility in UNIX. These fetched files are then READ though FORTRAN code developed for this project. Figure 3.4 depicts monthly data, obtained from our website http://www.arsc.edu/SpaceWeather/ .

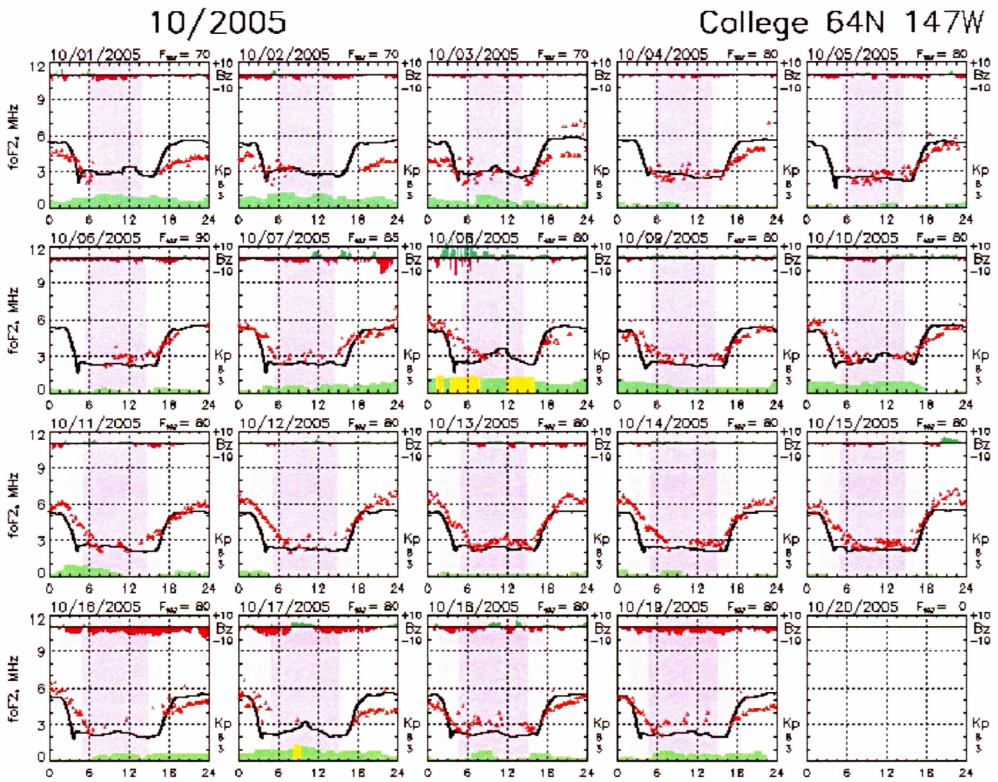

Figure 3.4 October 2005 measured vs. simulated results

3.7.2.3 Writing the Ionosonde Text File in Space Weather Format.

Various scaled ionospheric characteristics are then written into a text file similar to the NOAA Ionosonde format (ftp://solar.sec.noaa.gov/pub/lists/iono_day/). This subroutine runs in real-time and generates daily and monthly files for the GAKONA station. Then monthly plots are made available in real-time for the GAKONA station.

Chapter 4 GPS Total Electron Content Comparisons

4.1 The Global Positioning System

The GPS consists of 24 satellites that circle the Earth in 12 hour orbits These satellites have been launched and maintained by the department of defense (DOD) to provide all weather ranging 24 hours a day anywhere on the surface of the Earth. Each orbit is at an altitude of 20,200 km and contains four satellites. These satellites transmit two radio frequencies on two separate L-bands (L_1 = 1575.42 MHz and L_2=1227.60 MHz). The L_1 signal consists of a Course/Acquisition (C/A) and a Precision (P) code. The L_2 signal contains only the P-code. The L_1 and L_2 signals are available for military and other authorized users and provide a precise positioning service (PPS). The part of the GPS that consists of satellites is known as the space segment.

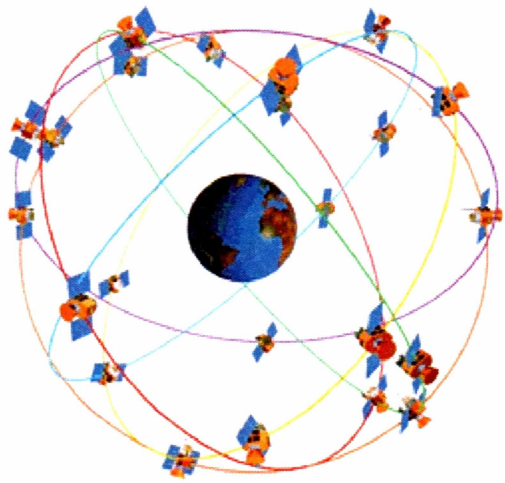

Figure 4.1 GPS Satellites (http://www.aero.org/education/primers/gps/whatisgps.html)

The user segment consists of GPS receivers that receive data from GPS satellites. The receiver computes the time required for the radio signal to reach the receiver from each of the satellites. From these timing signals, the receiver calculates its distance from each of the satellites by multiplying the time by the speed of the radio signal. In order to compute the position of a particular point, a GPS receiver needs at least positions of three satellites. However, the timing measurements are never completely accurate because the receiver clock is not as accurate as the atomic clocks in the satellites. The GPS receivers try to minimize timing errors using information from an additional (fourth) satellite. Although the GPS technology is quite involved, GPS users do not have to deal with the complexities of this technology. Users interact only with GPS receivers that are relatively simple to use. GPS receivers vary in both price and accuracy.

4.2 Principle of TEC Measurement using GPS

When a RF signal propagates through the ionosphere F-region, it is affected by certain disturbances like amplitude and phase scintillations of the signal. These scintillations can lead to degraded performance of communication or navigation systems, and even complete signal loss for the duration of scintillation activity. The Total Electron Content (TEC) in the signal's propagation path determines the magnitude of the time delay due to the ionosphere. TEC can be estimated by differential Doppler measurements, and also by measuring the amount of Faraday rotation of satellite signals. However, due to its wide usage and easy availability, the dual frequency GPS receiver system can provide an easy method to monitor the TEC globally by measurement of the relative

phase delay between the two working frequencies L_1 and L_2.

The parameter emulation software designed in this project is capable of calculating not only Slant TEC along the GPS signal path but also signal scintillations i.e., phase and amplitude scintillations. The ionosphere delays the phase and the envelope of the radio signals propagating through it. These delays have to be eliminated to obtain accurate positioning information from GPS signals. For precise measurements, two frequencies are used and the differential delay is calculated, from which the individual delays are determined. The differential delay so calculated can also be used to determine TEC as the delay is proportional to the integrated electron density. This TEC can be used to apply an ionospheric correction to the individual delays. Thus using the dual frequency GPS signal will yield accurate TEC measurements in addition to accurate positioning information.

4.3 TEC Measurement by using Group Delay

The ionosphere is a dispersive medium, and its refractive index n is a function of operating frequency, whose first order form can be expressed by Equation 4.1

$$n = 1 - \frac{Ne^2}{2\varepsilon_0 m\omega^2} = 1 - \frac{f_n^2}{2f^2}, \tag{4.1}$$

where N is the electron density, e is the electron charge (-1.602×10^{-19}C), ε_0 is the free space permittivity, m is the mass of the one electron (9.11×10^{-31} Kg), ω is the operating frequency in radians $\omega = \omega(f)$ i.e. $\omega = 2\pi f$, f is the operating frequency, and f_n is the

critical plasma frequency defined by $f_n = \sqrt{\frac{Ne^2}{\varepsilon_0 m}}$. This equation is from Komjathy [1997].

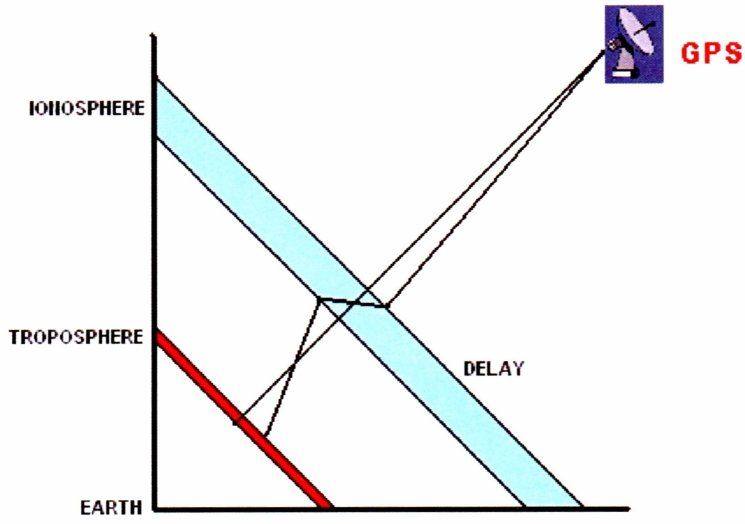

Figure 4.2 TEC calculation using group delay method

Range error due to time delay can be described as below

$$\Delta r = \Delta tc = \int (1 - n) dl \,. \tag{4.2}$$

From Equation 4.1, the range error is caused by the plasma refractive index, which is determined by the ionospheric plasma density N that varies with height and time. By combining Equations 4.1 and 4.2, we get the relationship between TEC and range error,

$$\Delta r = \int (1-(1-\alpha(f)))dl = \alpha(f)\int Ndl = \alpha(f)TEC\,, \tag{4.3}$$

in which $\alpha(f) = \dfrac{e^2}{8\pi^2\varepsilon_0 m f^2} = \dfrac{40.28}{f^2}$ is a constant determined by the system operating frequency.

GPS has two working frequencies, which can be used to get differential ionospheric time delay $\delta(\Delta t)$ as below,

$$\delta(\Delta t) = TEC\,\frac{\alpha(f_2)-\alpha(f_1)}{c} \tag{4.4}$$

in which $f_1 = 1575.42MHz$ (L_1 band) and $f_2 = 1227.60MHz$ (L_2 band).Thus TEC can be obtained from measurement of the group delay difference of GPS signals as below,

$$TEC = \frac{c\delta(\Delta t)}{\alpha(f_2)-\alpha(f_1)} = 2.854\times 10^{25}\,\delta(\Delta t)\left[\frac{electrons}{m^2}\right]. \tag{4.5}$$

If $\delta(\Delta t)$ is in *nano sec,* and TEC is in TEC Unit $TECU = 10^{16}\left[\dfrac{electrons}{m^2}\right]$, then

$$TEC\ [TECU] = 2.854\delta(\Delta t)\ [nano\,\sec].$$

The time delay difference between L_1 and L_2 provides a way to get a measurement of absolute TEC. Some of these equations are derived in Lettinger et al. [1975] and

Komjathy [1997].

4.4 TEC Measurement by the Carrier Phase Advance Method

From Equation 4.3, the phase advance due to the ionosphere can be represented by

$$\Delta\phi = 2\pi f \Delta t = \frac{2\pi 40.28}{cf} \int Ndl = \frac{8.44\times10^{-7}}{f} TEC\,[\frac{radians}{\sec onds}]. \qquad (4.6)$$

The differential carrier phase advance can be measured at the receiver by phase comparison of signals from two frequency GPS receivers. Two operating frequencies can give a differential or relative carrier phase advance, which is shown in Equation (4.7)

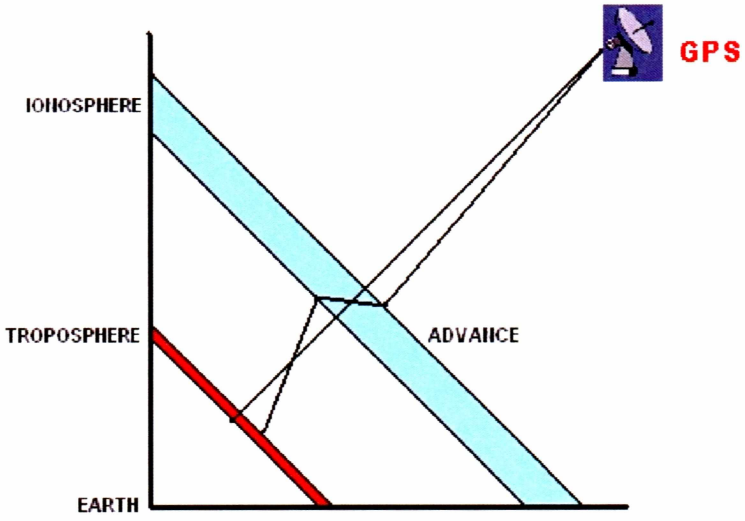

Figure 4.3 TEC calculation using phase advance method

$$\delta(\Delta\phi) = \Delta\phi_2 - \Delta\phi_1 = 8.44\times10^{-7} TEC\left(\frac{1}{f_2 - f_1}\right) = 0.17985\times10^{-16} TEC\,, \qquad (4.7)$$

where units are measured in radians/sec, Slant TEC is given by

$$STEC = 9.509 \times 10^{16}\ \delta(\Delta\phi).$$

Measurements of the differential carrier phase advance provide another way to obtain the TEC value. However due to ambiguity of the measurement on the number of differential phase cycles, this kind of measurement can only give the precise changes in the relative TEC.

4.5 Irregularities in the Ionosphere

Measured Total Electron Content depends on the irregularities in the ionosphere. This section describes the significance of such irregularities

4.5.1 Doppler Shift

The change in the frequency due to rapid changes in TEC and receiver's motion causes Doppler shift of the signals, which can be represented by the Equation 4.8 [Lettinger et al., 1984].

The rate of change of phase due to the change of TEC is

$$f_{Doppler}[Hz] = \frac{1.34 \times 10^{-7}}{f} \frac{d(TEC)}{dt} \left[\frac{TECU}{\sec} \right]. \qquad (4.8)$$

A rapid variation of TEC can result in a phase shift, which causes a spectral

broadening of the signal. For a stationary receiver, an upper limit of rate of TEC change is $0.1\times10^{16}\left[\frac{electrons}{m^2\,\sec}\right]$ per second can give a frequency shift of 0.085 Hz at L_1 and 0.109 Hz at L_2.

4.5.2 Faraday Rotation

Faraday rotation can be defined as the rotation of the wave polarization while propagating through the medium. It does not affect GPS satellite systems as they use circular polarization, but has loss effects for linearly polarized satellite systems, which can be predicted and compensated by the TEC measurement using Equation (4.9)

$$\phi = \frac{2.36\times10^4}{f^2} B\cos\theta\sec\lambda\cdot TEC\,, \tag{4.9}$$

where B is the magnetic field strength (W/m^2), f is the frequency in Hz, θ is the angle between the radio-wave normal and magnitude field direction, and λ is the angle between the wave normal and vertical [Hofmann, 1997].

4.5.3 Amplitude Scintillation

As we discussed earlier, irregularities in the ionosphere causes RF signal fading which leads to scintillations in the amplitude of the signal known as amplitude scintillations. Amplitude scintillations are caused by short-term signal fading due to irregularities of in Earth's ionosphere. Amplitude scintillations may cause the signal level

to fade below the receiver's lock threshold, which results in the receiver loosing track of the satellites. Usually the equatorial areas have severe signal scintillations that are strong after sunset until midnight. A GPS receiver can monitor amplitude scintillation by using the index S_4. First the signal is sent through a low-pass filter to get the normalized S_4 index, including ambient noise

$$S_4 = \sqrt{\frac{\langle P^2 \rangle - \langle P \rangle^2}{\langle P \rangle^2}} . \tag{4.10}$$

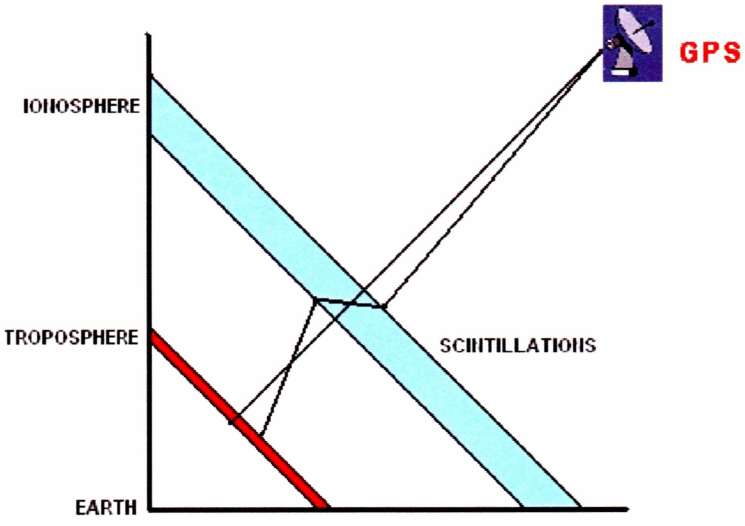

Figure 4.4 Scintillations in the ionosphere

Figure 4.4 demonstrates the method of estimation of scintillation parameters. The normalized power output of the low-pass filter can be written as

$$P_k = \frac{(NBP - WBP)_k}{(NBP - WBP)_{lpf,k}}, \tag{4.11}$$

where NBP and WBP are the narrow band and wide band power respectively, measured over the filter band interval every 20 milliseconds, where

$$WBP = \sum_{i=1}^{20} I_i^2 + Q_i^2 \quad \text{and} \tag{4.12}$$

$$NBP = \left(\sum_{i=1}^{20} I_i^2 \right)^2 + \left(\sum_{i=1}^{20} Q_i^2 \right)^2,$$

where I_i and Q_i are the 1 kHz in-phase and quadra-phase samples. The effects of ambient noise are then removed from the S_4 value and the final value for the S_4 index is derived from

$$S_4 = \sqrt{\frac{\langle P^2 \rangle - \langle P \rangle^2}{\langle P \rangle^2} - \frac{100}{\overline{S/N_0}} \left[1 + \frac{500}{19\overline{S/N_0}} \right]}. \tag{4.13}$$

These derivations are presented in Klobuchar [1983].

4.5.4 Phase Scintillation

Phase scintillation also occurs due to irregularities in the ionosphere. Phase scintillation occurs at the same time as amplitude scintillation due to small but rapid changes in the electron content of the ionosphere. The random component in severe phase scintillation will spread out the received signal. From Equation (4.10), if the TEC change is 0.19 TECU, there will be 1 radian of phase change at L_1, and 1 radian of phase change at L_2 corresponds 0.15 TECU of TEC change.

4.6 Emulation of Ionospheric Parameters - TEC and Scintillation Parameters

The major part of this project is to determine TEC and scintillation parameters of the ionosphere from the UAF ionospheric model and compare these to the GPS satellite data. Electron density values are obtained from the UAF Eulerian Parallel Polar Ionospheric Model. These values are obtained in real-time as a 3-D distribution on a regular computational grid. Slant TEC is obtained using integration of electron density selected along the signal path. Equation 3.21 is the basic equation for TEC estimation. A more detailed explanation of TEC estimation is discussed in Sections 4.5 and 4.6. TEC is estimated for all of the 24+ GPS satellites.

4.6.1 Geometry

Determination of geometric configuration is the major task for emulation of parameters of interest. TEC and S_4 computations are performed only when elevation angle is determined to be greater than 5 degrees, while elevation angle can be anywhere in the range [-90, 90].If the elevation angle is determined to be greater than 5 degrees, then azimuth angles as well as other parameters are determined. The coordinates are selected along the beam path and then TEC is estimated through integration.

4.6.2 Estimation of Scintillation Parameters

The S_4 Scintillation Index is defined in Section 3.5.4, and its estimation from model data is done using the complex phase method **(CPM)** [Gherm et al., 2005]. The CPM deals with the monopole field, rather than with plane wave propagation. It takes into

account the ray bending due to the inhomogeneous background ionosphere and the diffraction effects on local random ionospheric inhomogeneities. This method provides the possibility to simulate statistical characteristics of the ray pad for different geophysical conditions of propagation. The Complex Phase Method has been extended to study the problem of electro magnetic (EM) field scintillations on Earth-satellite GPS paths of propagation. When dealing with the scintillation effects, attention is paid to the behavior of phase and amplitude fluctuations, the scintillation index S_4, the type of statistics of the field fading. The relationship between GPS amplitude scintillation and TEC is referred to as GPS phase fluctuations. In this project, amplitude and phase scintillations are calculated using above mentioned method.

4.6.3 Programming Techniques

In this thesis software was developed for UAF ionospheric model validation, i.e., for making comparisons between measured data from HAARP and simulated results from the model. A major part of the code package is written in FORTRAN; various subroutines are developed for reading the input, writing the output, determination of geometric configuration, azimuth and elevation angle calculations, STEC and scintillation parameters estimation. UNIX shell scripts are developed as well for the various tasks of this code. Python scripts were developed to fetch the real-time HAARP NetCDF data files from the website. A C++ parser was also developed for this purpose. Graphical package IDL is used for plotting the TEC, S_4 and elevation angle values. This plot is updated daily at the UAF EPPIM webpage. It actually provides the comparison

between measured and simulated values.

4.6.3.1 Inputs to the Code

Inputs to the program are the current Cartesian coordinates of the GPS satellite. These are obtained from the GPS WWW-site http://igscb.jpl.nasa.gov/ through reading the SP3 format file with history and forecasts of GPS orbital position. The individual file covers the time interval of [-12, 12] hours with respect to current time. Cartesian coordinates of the receiving station are necessary as well as the ellipsoidal coordinates of the receiving station.

4.6.3.2 Operation of the Code

The basic operational steps of the code are:

1. Determination of the elevation angle of the individual GPS satellites and, if this elevation angle is greater than 5 degrees, further computation takes place. Otherwise all computable parameters in the output files are filled with dummy values (e.g., 999). Only if the elevation angle is greater than 5 degrees the code determines:
2. Azimuth angle.
3. Distance to satellite and parameters related to the crossing of ionospheric boundaries to facilitate proper CPM operation.
4. Electron density and slant TEC along the path.
5. Angle between the direction of propagation and the magnetic field vector along

the path.

4.6.3.3 Outputs from the Code

1. Elevation angle.
2. Azimuth angle.
3. Latitude and longitude of the beam crossing of the ionospheric F2-layer assumed at 350 km.
4. Latitude and longitude of the beam crossing of the ionospheric E-layer assumed at 120 km.
5. Amplitude scintillation, phase scintillation, cross correlation and scintillation index (S_4).
6. Total Electron Content in TEC units (TECU).
7. Electron density (Ne) at the individual locations along the path, recalculated into plasma frequency for CPM operation.

4.7 Comparison with UAF Ionospheric Model-Validation

The plot below in Figure 3.6 is the TEC vs. UT plot. GPS elevation angles are shown as black curves. Red curves depict TEC values measured at the HAARP site and green curves show TEC values emulated from the UAF EPPIM model. Scintillation index (S_4) is plotted as blue curves. PRN indicates the GPS satellite numbers. Figure 4.5 is the TEC and S_4 sample plot obtained from the HAARP webpage. The plots are updated daily in real-time and can be obtained at http://www.arsc.edu/SpaceWeather/s4.html.

Detailed descriptions of the comparisons are available from Lanyi [1988] and Sardon et al. [1995].

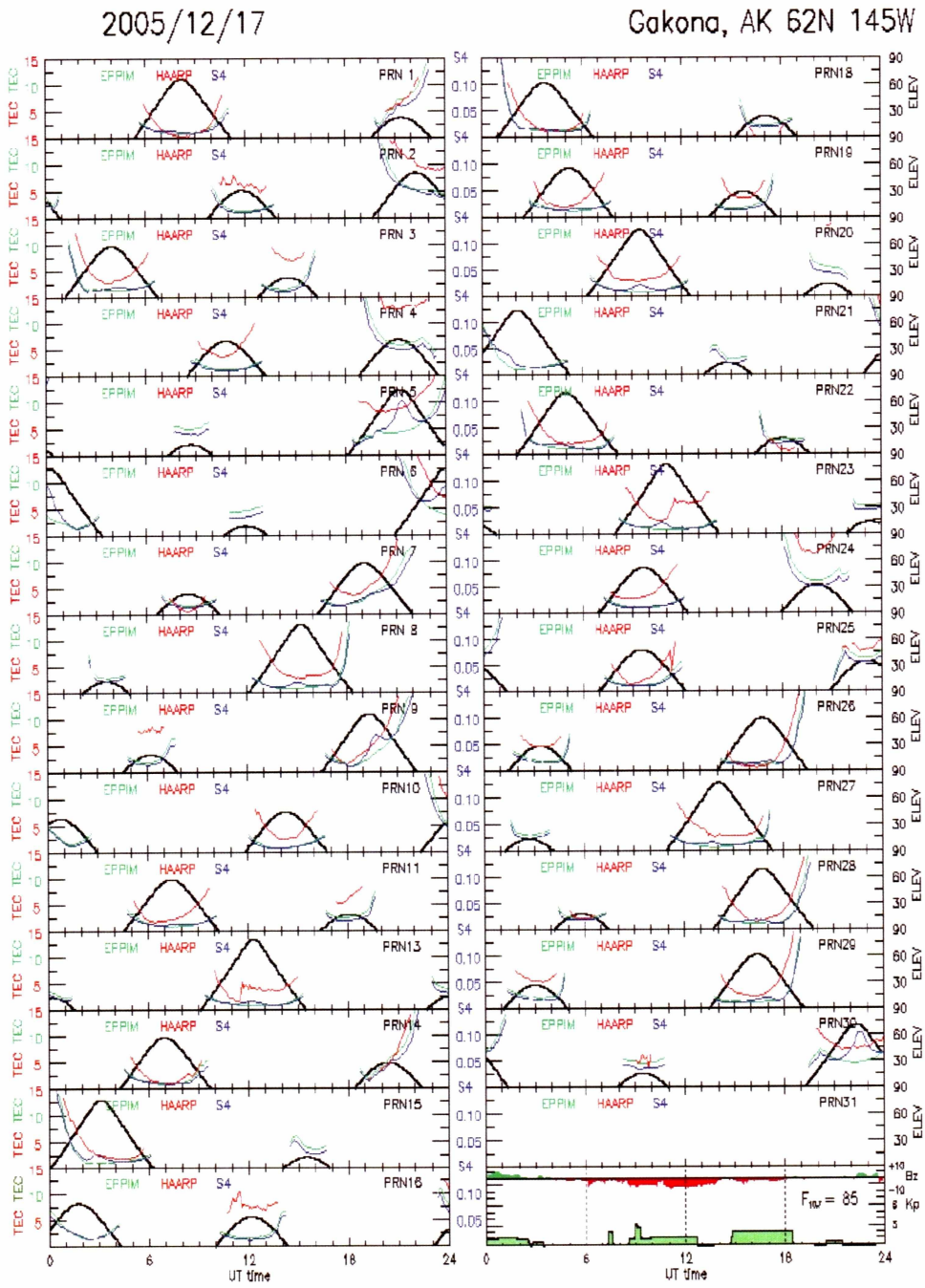

Figure 4.5(a) TEC comparison plot 2005/12/17

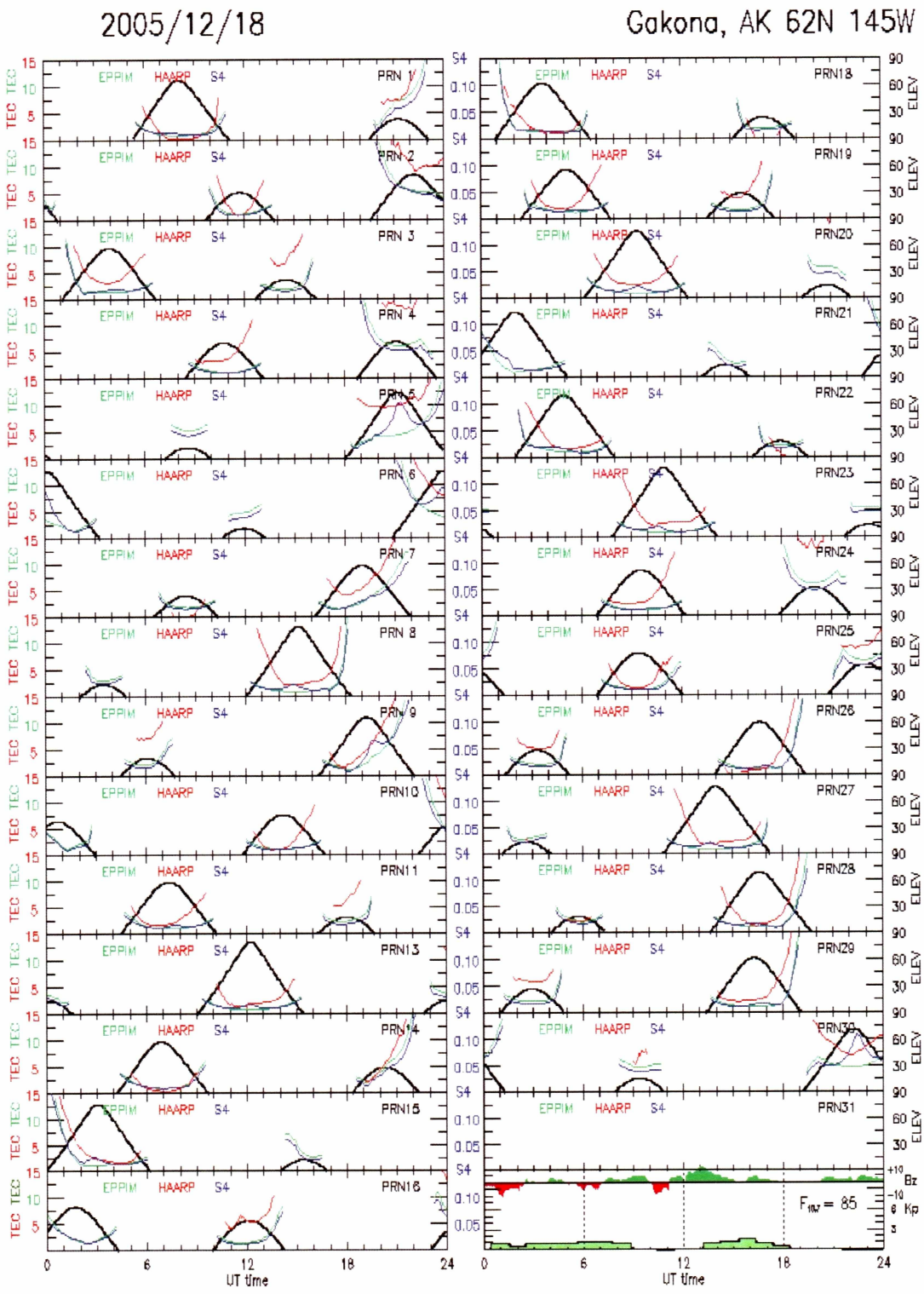

Figure 4.5(b) TEC comparison plot 2005/12/18

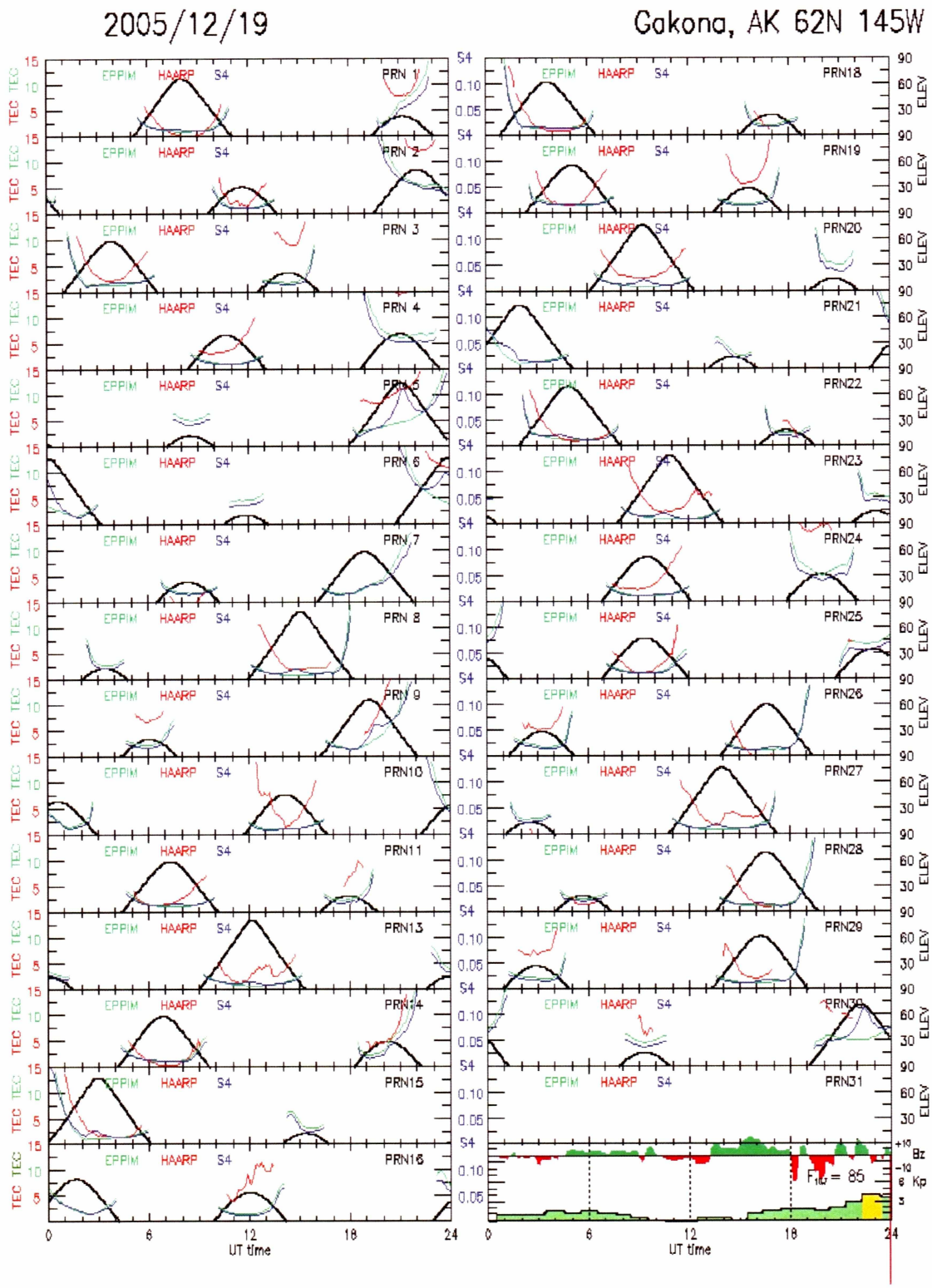

Figure 4.5(c) TEC comparison plot 2005/12/19

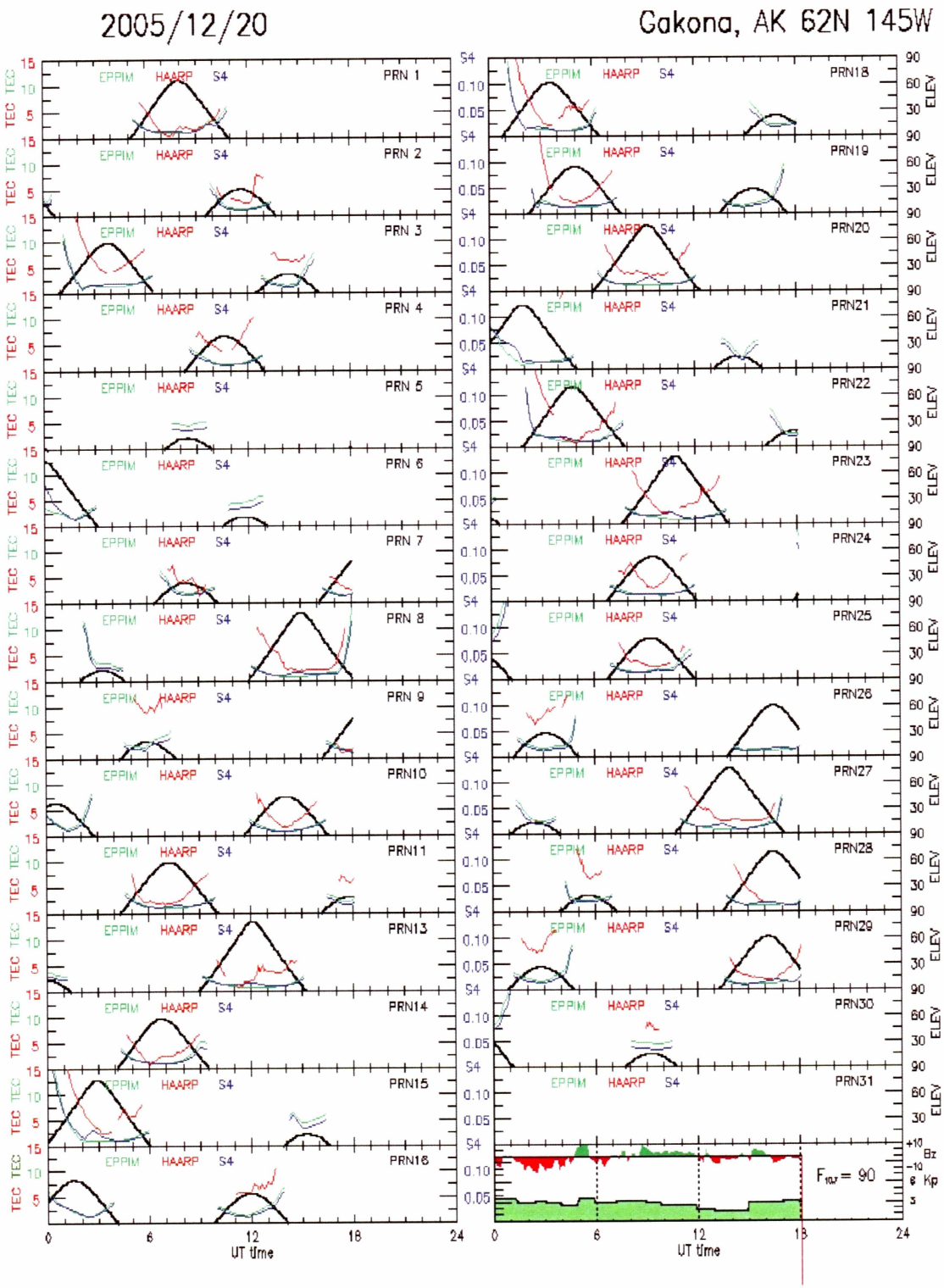

Figure 4.5(d) TEC comparison plot 2005/12/20

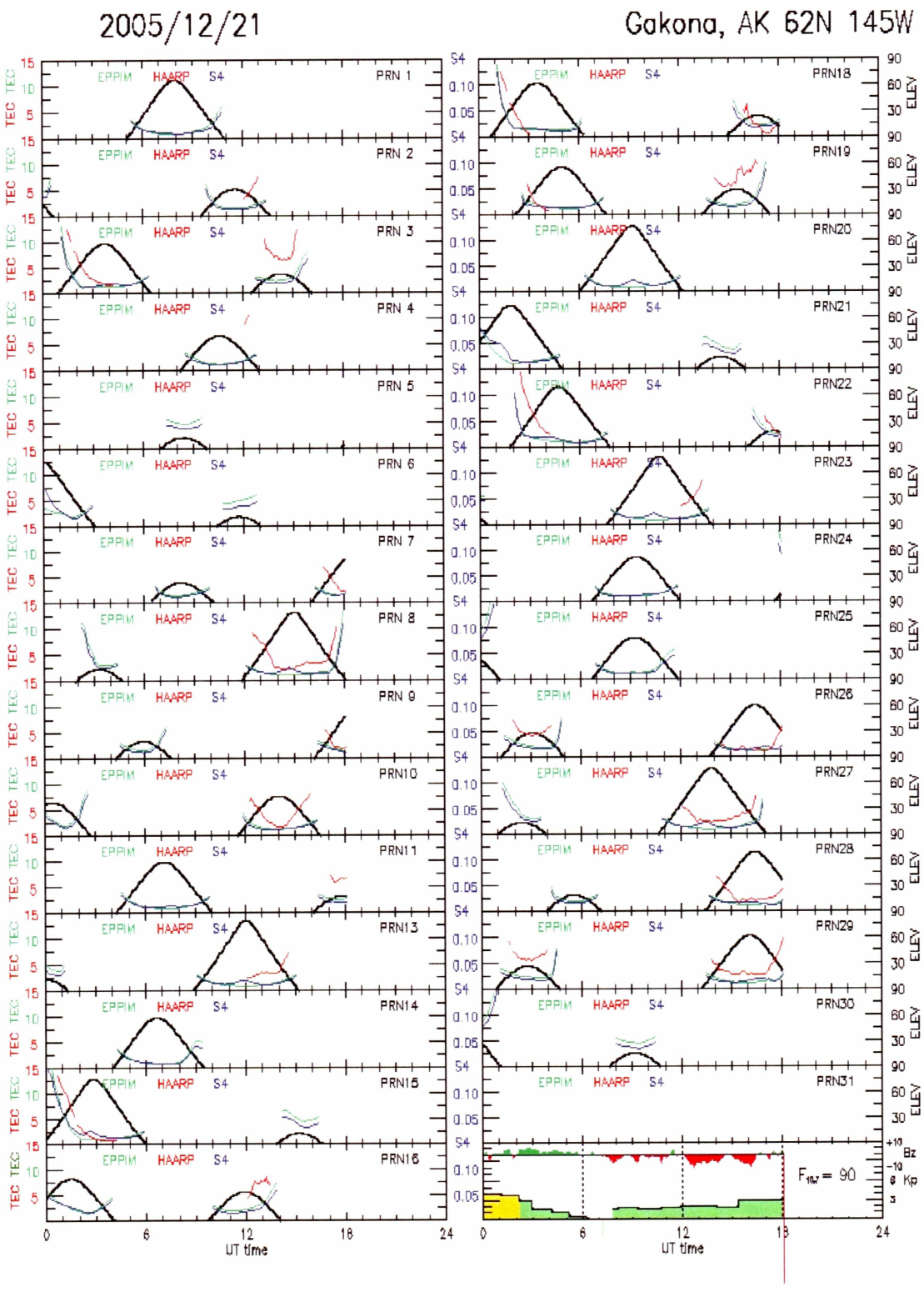

Figure 4.5(e) TEC comparison plot 2005/12/21

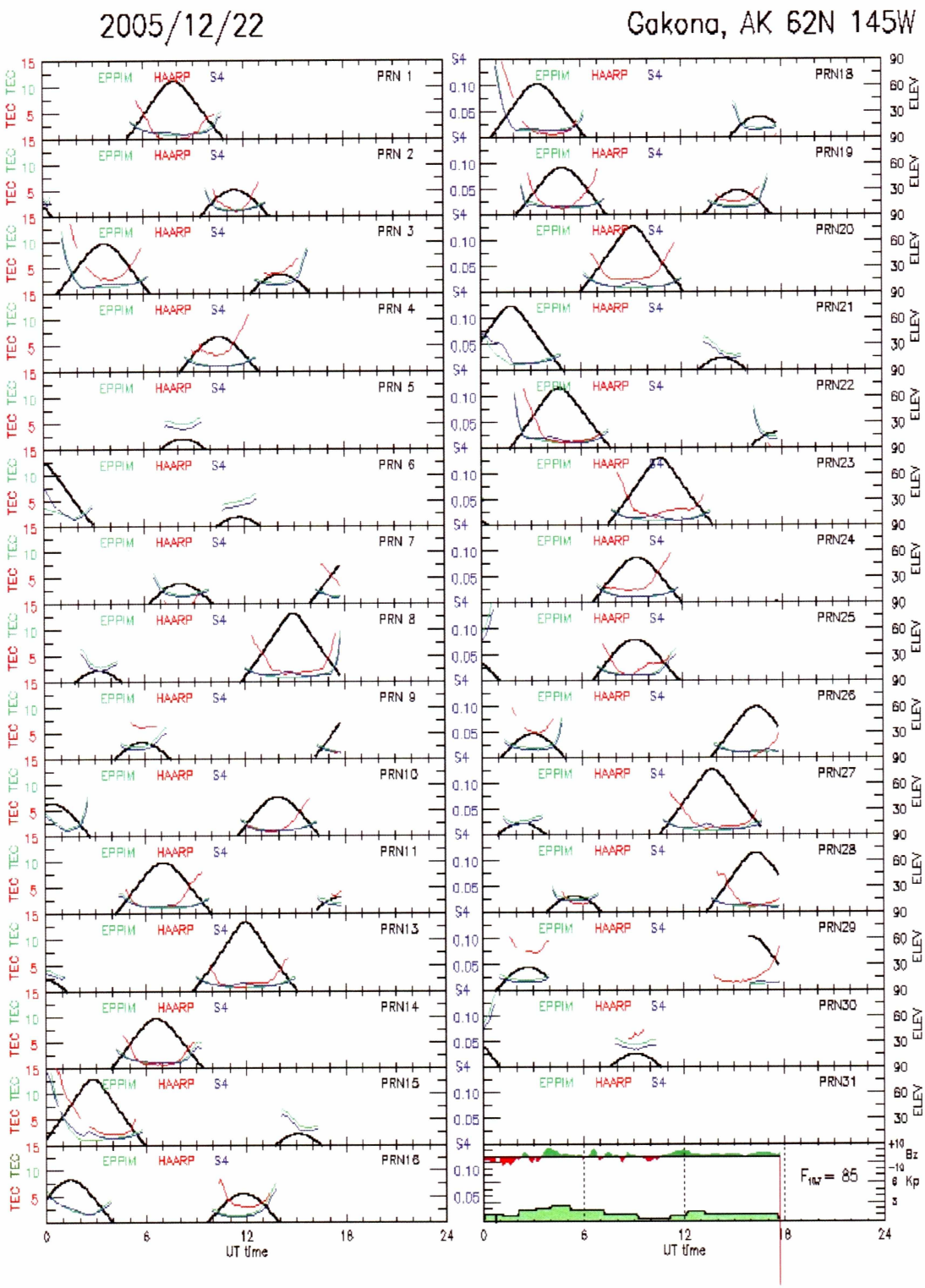

Figure 4.5(f) TEC comparison plot 2005/12/22

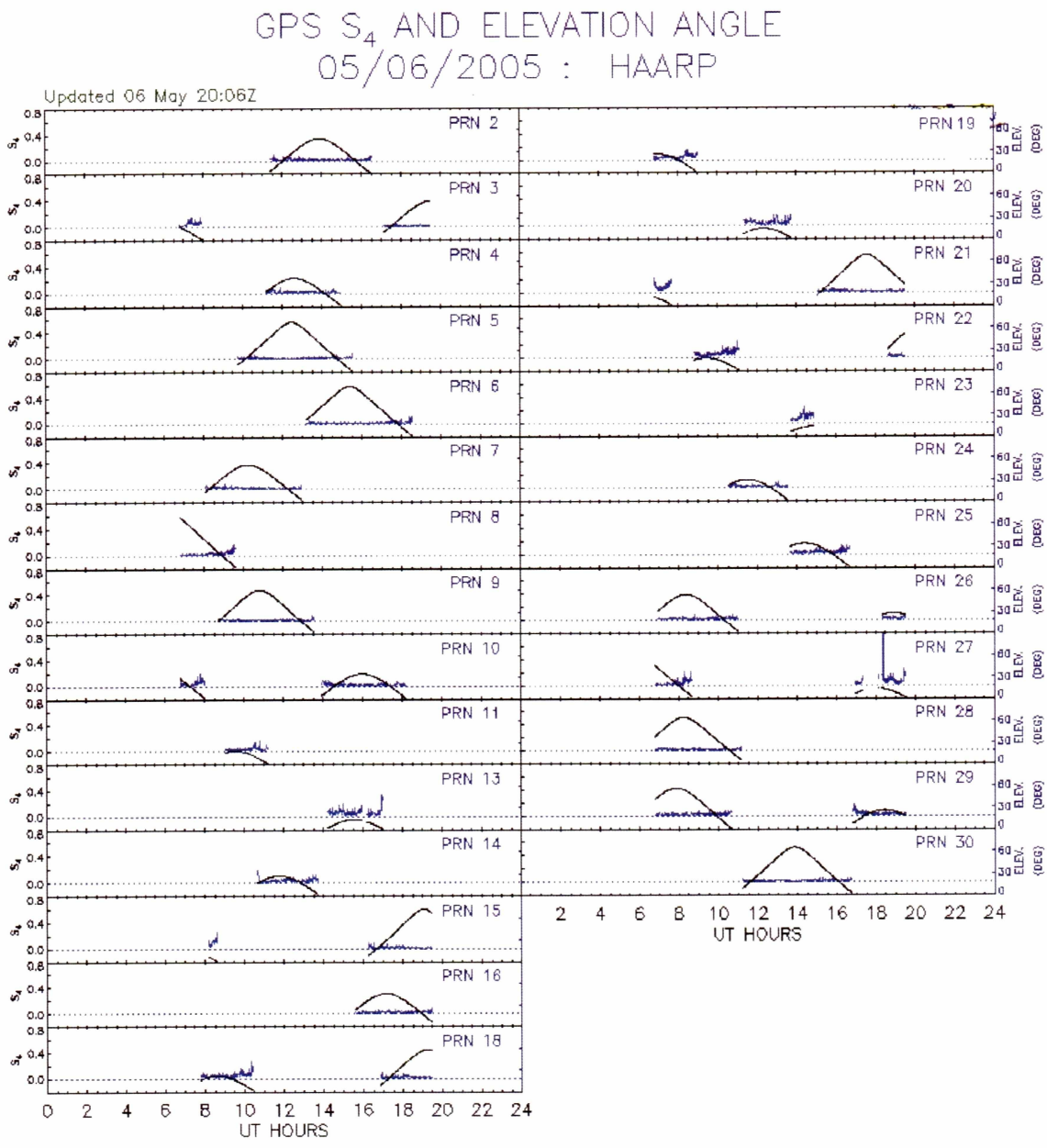

Figure 4.6 Scintillation index and elevation angle from HAARP database

4.7.1 Model Validation

To study the results, measured and simulated data are taken from 17th Dec 2005

to 22nd Dec 2005. Thus, on analysis of various plots of Figures 4.6, which compare simulated and measured results, we conclude that a tool for validation or validation capability of the model has been developed.

Chapter 5 Ionospheric Tomography

5.1 Ionospheric Tomography

"Tomography refers to the cross-sectional imaging of an object from either transmission or reflection data collected by illuminating the object from many different directions" [Austen et al., 1990].

Tomography consists essentially in reconstructing an *image* (in this case the 3D distribution of free electrons) from its *projections* (in our case the STEC), which are the integrals of the image in a given direction. The applications of this technique are extremely broad, from medical sciences to the mapping of underground resources. Ionospheric sounding using satellite data has also taken advantage of this technique to reconstruct the state of the ionosphere (by monitoring the distribution of its electron density). The first work that introduced the concept of ionospheric tomography is described in Austen et al. [1990], although further improvements and studies were performed in following works by many authors [Raymund, 1990] and [Fremouw et al., 1992].

Ionospheric tomography provides a high resolution image of the electron density distribution in the vertical, meridional plane using only a small number of satellite receivers on the ground. HAARP site provides access to the Total Electron Content tomographic data and signals received are measured at different ground stations. The

TEC along each ground satellite path is calculated. Fleming [1982] and Na [1991] demonstrated the basic concept of Ionospheric Tomography and its importance.

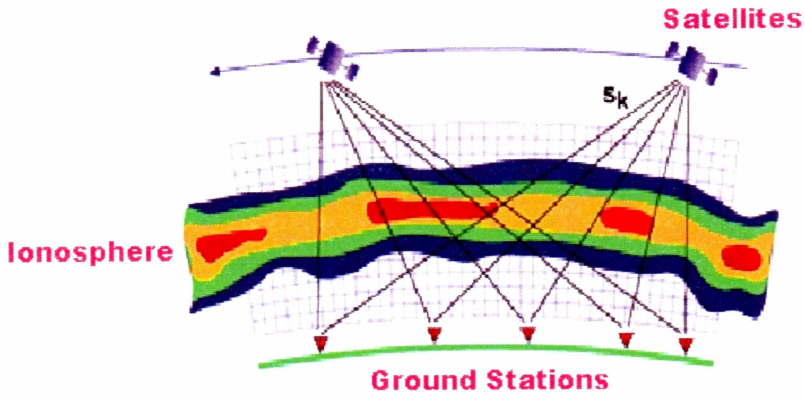

Figure 5.1 Geometry of ionospheric tomography experiment

Figure 5.1 describes the basic geometry of the Ionospheric Tomography, with Stations located on the surface of the Earth. [http://www.sgo.fi/Data/Tomography/tomoDescr.php]

5.2 Reconstruction Techniques

The reconstruction algorithms which are used for Computerized Tomography can be classified broadly in to two groups: transform methods and series expansion methods. The theory behind each of these will now be presented. The next section deals with the transform methods of reconstruction, followed by the limitations of ionospheric tomography techniques [Lewitt, 1983].

5.2.1 Reconstruction Techniques used at HAARP

Computerized ionospheric tomography (CIT) at HAARP is implemented by North West Research Associates (NWRA). NWRA is a scientific research group owned by its principal investigators, with experience in geophysical and related sciences. Stochastic (statistical) methods were used for ionospheric tomography reconstruction at HAARP. These methods were clearly demonstrated in Fremouw et al. [1992]. The topic of study is satellite radio tomography, and their analysis is based on stochastic inversion. The experimental method is difference Doppler measurement, which gives the phase difference of coherent radio waves at two frequencies. The waves are transmitted by a navigational satellite flying above a chain of receivers placed at ground level. The phase difference is proportional to the oblique ionospheric electron content, i.e., the integral of electron density along the ray from the satellite to a receiver. The result of inversion is electron density in the orbital plane of the satellite.

Stochastic inversion greatly differs from all iterative methods. The most important difference is that stochastic inversion has a firm mathematical background. Therefore it is well understood what the result actually is; it simply gives the most probable values of the unknowns once the measurements are known and the regularization is fixed. The effect of measurement errors is also included in the formalism. An important part of stochastic inversion is regularization which prevents non-physical point-to-point oscillations otherwise created by the numerical instability in matrix inversion. As described in Fremouw et al. [1992], a two dimensional (altitude and geomagnetic

latitude) electron density field is represented by means of two dimensional basis functions and corresponding coefficients. This transforms the problem into estimation of model vector **m** and its corresponding elements. The linear relation between vector of measurements and vector of unknowns is

$$\mathbf{d} = G \cdot \mathbf{m} + \mathbf{n}, \tag{5.1}$$

where G is the geometry matrix describing the dependence of data on model parameters and **n** is the noise vector. With the forward problem formulated as in Equation 5.1, the inverse problem becomes that of solving the equation for an estimated model vector, $\hat{\mathbf{m}}$, employing a generalized inverse matrix, G^{-g}, as follows:

$$\hat{\mathbf{m}} = G^{-\mathbf{g}}\mathbf{d}, \tag{5.2}$$

as described in Section 2.3 of Fremouw et al. [1992], we employ

$$G^{-\mathbf{g}} = \mathbf{v}G^T(G\mathbf{v}G^T + \mathbf{e})^{-1}, \tag{5.3}$$

where **v** and **e** are the a priori covariance matrices of **m** and **n**. In practice, covariance matrices are taken as diagonal, so they become variance vectors. In this theory, two important considerations arise: the choice of basis functions and the weights to assign to

them in defining the a priori variance vectors **v** and **e.** Substituting Equation 5.2 in 5.3 produces

$$\hat{\mathbf{m}} = G^{-\mathbf{g}} G\mathbf{m} + G^{-\mathbf{g}}\mathbf{n}. \tag{5.4}$$

In this analysis, the vertical plane is divided into a rectangular grid (in geocentric spherical coordinates), and the electron densities at the grid points as well as the unknown phase constants are the unknown quantities. Bilinear interpolation inside each mesh of the grid is used in calculating the integrals.

5.3 Limitations of Computerized Ionospheric Tomography

Although tomography has great potential, the inherent geometry involved in the ionospheric case (i.e. it is not possible to have observations in all angles), the location of the receivers used and the discrete nature of the data impose certain limitations as pointed out in [Austen et al., 1998]. These limitations applied to ionospheric tomography with GPS can be summarized in two issues: (1) Lack of vertical resolution (2) Sparsity of data.

5.3.1 Lack of Vertical Resolution

Satellite ionospheric tomography using ground receivers presents the problem of the vertical resolution. Although good estimates of vertical TEC can be achieved, it is very difficult to distribute the electron content properly in the different layers of the vertical. This is due to the fact that satellite slant TEC observations gathered by ground receivers do contain vertical information but to a very limited extent, which is not enough

to decompose the integral to obtain the different contributions of the electron density. In this context, several solutions are devised.

5.3.2 Sparsity of Data

Although the number of operational GPS receivers has been increased in recent years, the GPS receiving stations are unevenly distributed on the Earth. Density of these receivers is much less in Africa, compared to Europe and America. These unevenly distributed GPS receivers means that those regions with a high density of GPS receivers can image the ionosphere properly. On the other hand, those regions with a lack of receivers generate areas where the ionosphere is difficult to monitor. In order to solve this problem, interpolation techniques become essential. The interpolation scheme may be aided with the use of a model, as in the case of polar vertical TEC maps computed in the UAF Ionospheric model, where the interpolation aided by the IRI model was used to deal with this issue.

5.3.3 Improving System Geometry

In this project, data taken is from GPS and other geostationary satellites. These satellites, when in conjunction with ground based receivers, do not improve the geometry of the acquisition system, but rather present some additional drawbacks. Improvements to the system geometry, on the other hand, could come from what is technically called *occultation,* i.e., measurements where both the transmitter and receiver are located on satellites. A typical example is the occultation between low Earth orbit (LEO) satellites

and GPS satellites. LEOs, which orbit at about 800 km of altitude, are equipped with GPS receivers. The lines of sight between a LEO and a GPS satellite provide the user with a vertical ionospheric profile, every time the LEO satellite appears or disappears behind the horizon of the GPS satellite. Using a 3D reconstruction geometry, like the one we are proposing, alignment of GPS and LEO in the plane where the other TEC measurements lay (approximately in the case of linear array of ground receivers) is not even required.

5.4 TEC Tomography at the HAARP

In this thesis, real-time comparisons of TEC tomography are done by comparing the TEC tomography obtained from the HAARP facility with the outputs obtained from the UAF Polar Ionospheric Model. The most recent image obtained from the HAARP site is compared with the most recent image of the Model. Electron Density Ne is plotted along the altitude. Total Electron Content is determined by taking the line integral of electron density.

5.4.1 High Frequency Active Auroral Research Program (HAARP)

HAARP is a DoD owned upper atmospheric research station located in Gakona, Alaska. It contains high power, high frequency phased array radio transmitter which is used to heat the ionosphere at particular heights. This instrument shown in Figure 5.2 is used to study the polar ionosphere. HAARP also has ultrahigh frequency (UHF) incoherent scatter radar (ISR), which is used to measure electron density in the ionosphere. This facility is operated by DoD to study the upper atmosphere.

Figure 5.2 HAARP phases array transmitter

5.4.2 Image Reconstruction

The most fundamental parameter describing the ionosphere is electron number density, Ne (electrons/m^3). Its line integral is termed total electron content (electrons/m^2), or TEC. Medical tomography results from mathematical inversion of line integrals of some parameter of interest, obtained for instance along many x-ray paths. Using similar techniques, we can produce tomographic images of the ionosphere from TEC measurements made at a latitudinal chain of ground stations during flights of polar orbiting satellites that transmit appropriate radio waves. A tomographic image obtained from the HAARP website is shown in Figure 5.3. The reconstructed tomographic image was obtained in real time, with varying altitude and geomagnetic latitude along the Y and X axis, respectively. Cordova, Gakona, Big Delta, Fort Yukon, Kaktovik are different HAARP stations shown along the geomagnetic latitude. The tomographic image is

reconstructed by taking a horizontal slice from North to South along these four different stations.

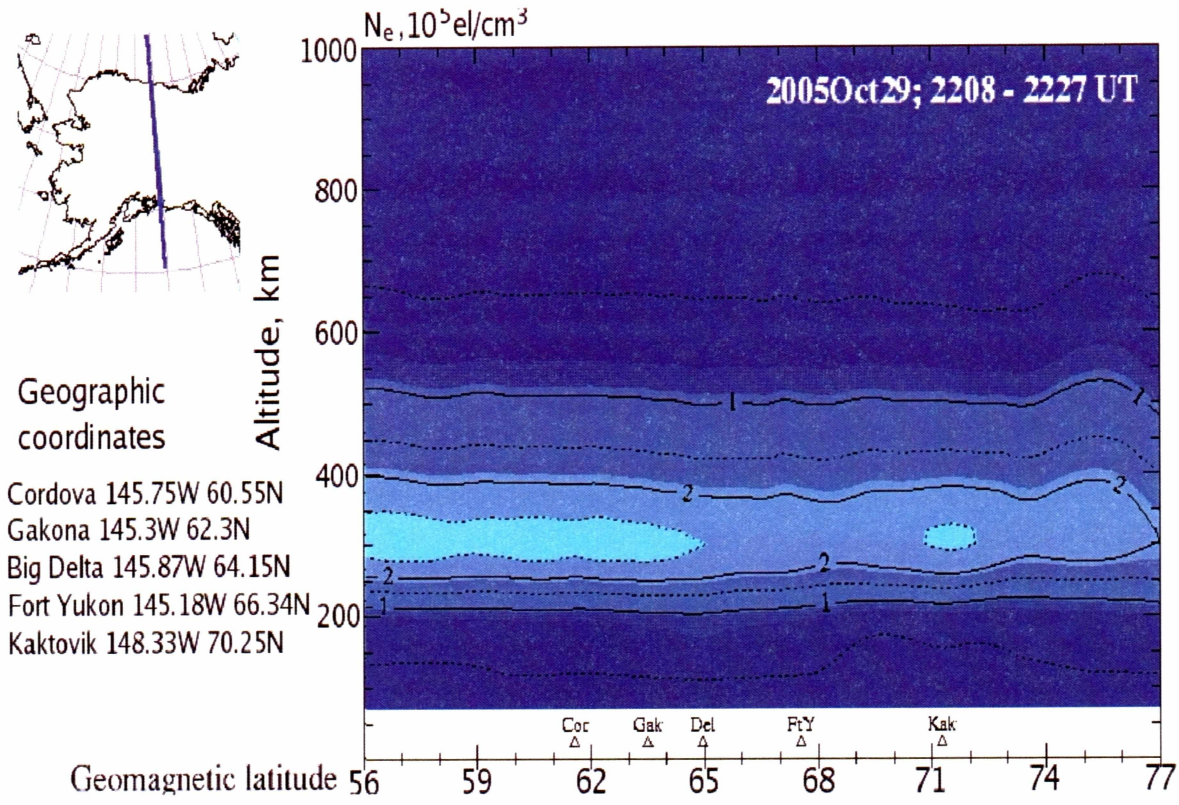

Figure 5.3 Tomographic image of the ionosphere

5.5 TEC Tomography from the UAF Ionospheric Model

For the tomography reconstruction, a blade utility was developed. The major task of this utility is to get the exact slice from the model (UAF EPPIM) data file along the circle between two points on the globe. Code is written in C++. The main program writes a file with sliced data and the data are then interpolated from provided input. Later GNU Plot

was used to prepare the comparison plots. The horizontal line (in reference to Earth) shown on the Alaska map in Figure 5.4 is the slice taken to reconstruct the tomographic image.

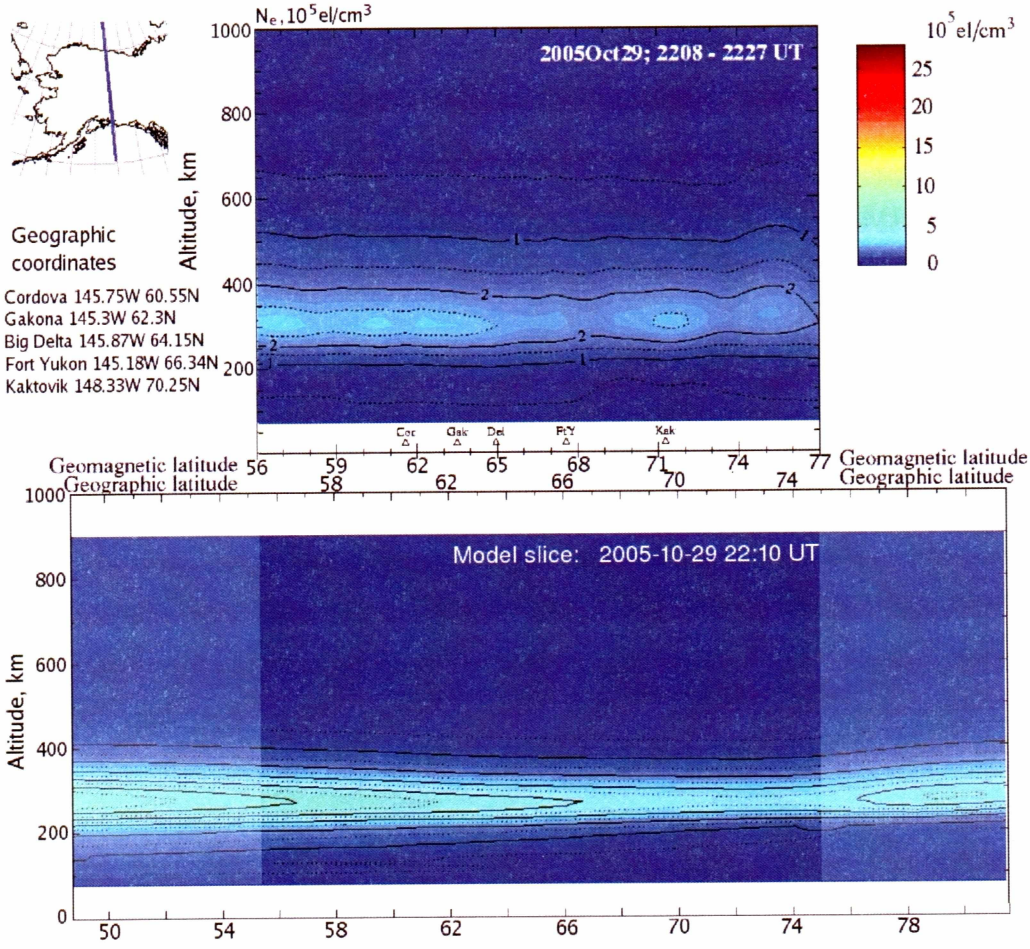

Figure 5.4 UAF polar ionospheric tomography snapshot

This image was obtained in real-time and published on our website. This link is http://ion.gi.alaska.edu/index.php?item=comparisons_tomo.

Real-time comparisons of TEC tomography were done by comparing the TEC tomography obtained from the HAARP facility with the outputs obtained from the UAF

EPPIM model. The most recent image obtained from the HAARP site was compared with the most recent image of the model.

5.5.1 Validation Capability

By analysis of simulated and measured results, a validation capability for the UAF EPPIM has been developed using this computerized ionospheric tomography software.

5.6 Programming Techniques

Initially the latest images were downloaded from HAARP website. These images were downloaded using a Python script. HTML parsing was done to retrieve the images from the website. This image was inserted into the database using insert_images.py. These images were stored in the database. The main part of the tomography comparison system is tomo.py script. This script does the following operations:

- Initially it checks the name of the last HAARP experimental tomography slice available on-line.
- If the ionosphere tomography picture already exists in the database, then it won't download. If the picture is new, compared to the picture downloaded before, then tomo.py downloads this new picture.
- After downloading the latest image, Script selects the model slice picture from the database for the appropriate time. This time is determined from the HAARP picture's filename.

- tomo.py then combines the model slice and the HAARP tomography picture into one comparison picture.
- Finally, tomo.py inserts the comparison picture into the database.

Cron runs the tomo.py script from the scratch/scripts/tomography directory every 30 minutes. It is scheduled under user realtime crontab.

Chapter 6 Software Development

In this chapter a summary of the software and its functions that have been developed for this thesis project are presented. Two new software methods have been developed to provide a validation capability for the UAF Eulerian Parallel Polar Ionospheric Model. These techniques are:

- TEC emulation using GPS satellite data.
- Computerized ionospheric tomography.

These techniques are very useful because,

- Real-time validation can provide much information about the model quality, determine its limitations and define the directions of improvement.
- Real-time comparisons help to determine trusted intervals for the model parameters for future data assimilation tasks. In this case real-time comparisons are of forecast model capability.

6.1 TEC Emulation Using GPS Satellite Data

The software developed calculates the GPS satellite position, GPS time with respect to standard time (UT), Total Electron Content, elevation and azimuth angles and scintillation parameters. Calculation of TEC using GPS satellites is described in Chapter 4 of this thesis. This chapter describes the software development that calculated the parameters and results as shown in Figures 4.5 (a) to 4.5 (e). In this thesis software was developed for the purpose of validating the UAF ionospheric model i.e., for making

comparisons between measured ionospheric data from the HAARP site and simulated results from the model.

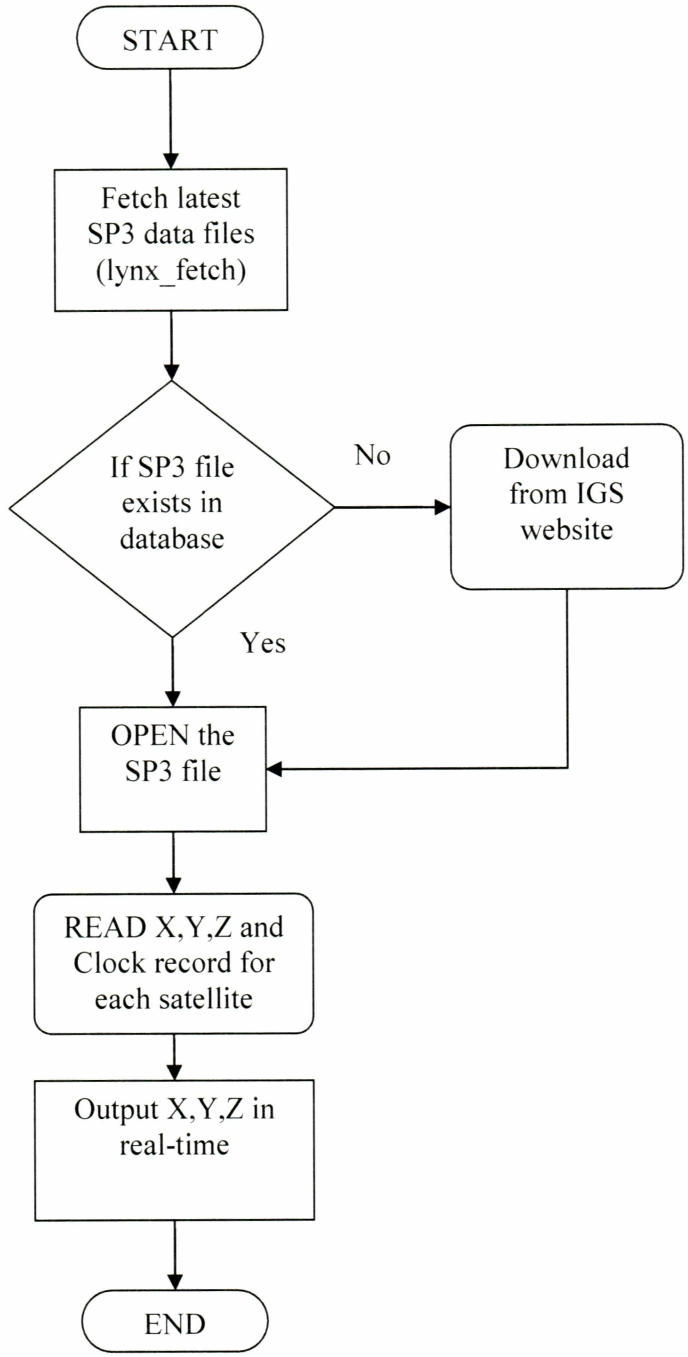

Figure 6.1 Subroutine to calculate the position of each GPS satellite

6.1.1 Calculation of the Position of each GPS Satellite

The algorithm for Cartesian coordinates calculation is shown in Figure 6.1. This program initially fetches SP3 format GPS satellite data files from the International GPS service website (http://igscb.jpl.nasa.gov/). Lynx, a UNIX utility, is used to fetch the real-time data from the web site. A UNIX shell script is developed which checks and downloads the latest SP3 format files in to the directory. FORTRAN code is developed which opens the SP3 format text file and reads the Cartesian coordinates of each GPS satellite. The (x,y,z) coordinates are available as outputs. After determining the position of each GPS satellite, the elevation angle is determined for each GPS satellite with respect to the ground plane; more detailed explanation is given in Chapter 3 of this thesis.

6.2 TEC Emulation Using Subroutine GPS_parameters.f

The subroutine *GPS_parameters.f* emulates and outputs the STEC, S_4, orbital geometry (elevation and azimuth angles) and electron density along the GPS satellite path. These parameters are determined for all the GPS satellites and then finally compared with the measured data from HAARP web site. Positions of each GPS satellite are the inputs to this subroutine. 3-D electron density values are also taken as inputs from the UAF EPPIM. Elevation angle of the GPS satellite with respect to an observer on the Earth's surface is calculated. If the GPS satellite is visible from the receiving site (elevation angle greater than 5 degrees), the code determines azimuth angle and then it calls subroutine *index_feeder.f* which selects proper 3-D Ne elements into a 1-D array along the satellite path. Subroutine cart_2_spher.f is shown in Figure 6.3, which converts

Cartesian coordinates (x,y,z) to spherical coordinates latitude, longitude and ellipsoidal height. Finally slant TEC and Scintillation Index are calculated.

This subroutine provides output files (YYYYMMDD_GPS_EPPIM.txt) in text file format. YYYY indicates current year, MM indicates month and DD indicates current day, for example *20060206_GPS_EPPIM.txt* is a sample output file. This file contains azimuth and elevation angles of each GPS satellite, its corresponding STEC, latitude and longitude crossing E and F2 layers and scintillation parameters. This code calculates and outputs parameters for all the 31 GPS satellites, shown as PRN in the algorithm which indicates satellite number. The DO loop runs from PRN 1 to PRN 31 and calculates parameters for a particular universal time. Latitudes and longitudes of the beam crossing the ionospheric E-layer and F2-layer are also calculated from this software. This software runs in real-time, i.e., it fetches files from the website in real-time, computes the parameters and outputs them in real-time. Plotting is done using graphical package IDL, where measured and simulated TEC, S_4 and elevation angles are plotted.

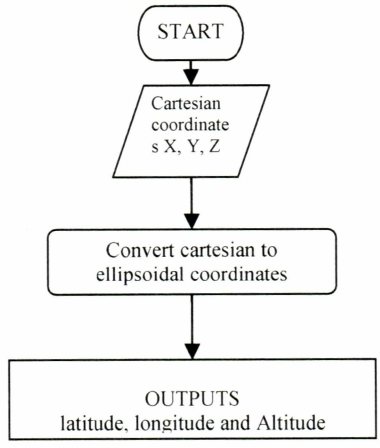

Figure 6.2 Subroutine cart_2_spher.f

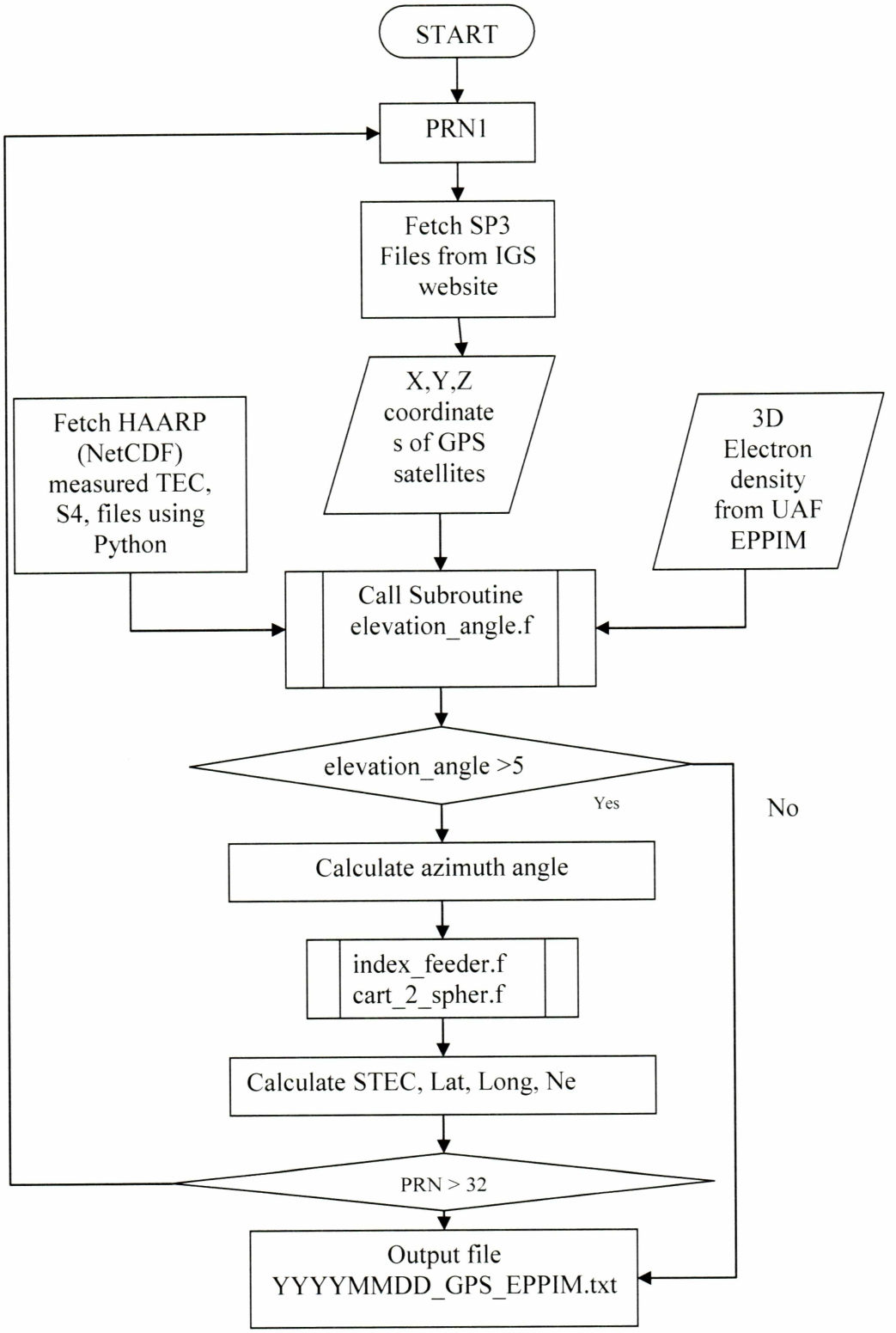

Figure 6.3 Subroutine GPS_Parameters.f

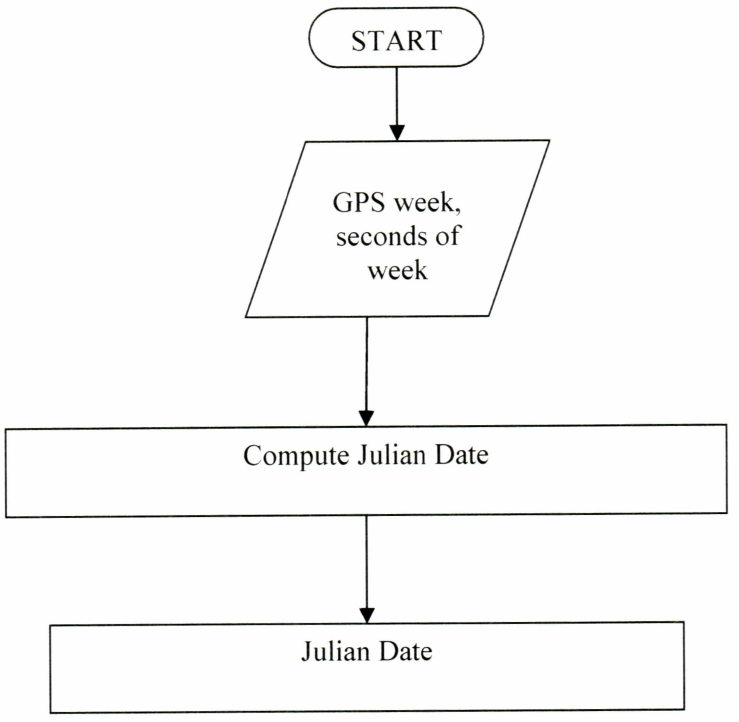

Figure 6.4 Subroutine to calculate Julian date

This subroutine *gps2jd.f* takes the GPS week number beginning with 0 (starting on Jan 1980) and also takes the seconds of the week and computes Julian date. Then, GPS time is determined. This GPS time is important as the software developed is for real-time validation. By knowing the GPS time, we can determine the exact time of each GPS satellite.

6.3 Ionospheric Tomography

Comparisons of ionospheric model outputs with ionospheric tomography outputs is the second new tool developed to provide a validation capability of UAF EPPIM. C++,

C, Python, PHP and mySQL have been used in the various stages of this model development. In the process of this software development, a real-time management system (RMS) has been developed; this model prepares the 2-D tomography images from 3-D electron density values and also prepares the comparisons plots discussed in Chapter 5. For comparisons with ionospheric tomography, a utility called *blade* was developed; the major task of this utility is to get the exact slice from the model (UAF EPPIM) data along the great circle between two points on the globe. Code is written in C++. The main program writes a file with data for a 2D slice interpolated from the model 3D distribution. A Python script tomo.py is developed to perform the following tasks:

1. All of the latest ionospheric tomography images are downloaded from the HAARP website using this script; these images are stored in the database.
2. The script checks the name of the latest HAARP experimental tomography slice available on-line.
3. After downloading the latest image, the script selects the slice picture from the model database for the appropriate time. This time is determined from HAARP picture's filename.
4. Then the model slice and the HAARP tomography picture are combined into a single comparison picture.
5. Finally, the script inserts the comparison picture into the database for WWW-access.

These resultant images from the above process are available at the UAF EPPIM website (http://ion.gi.alaska.edu/) in real-time.

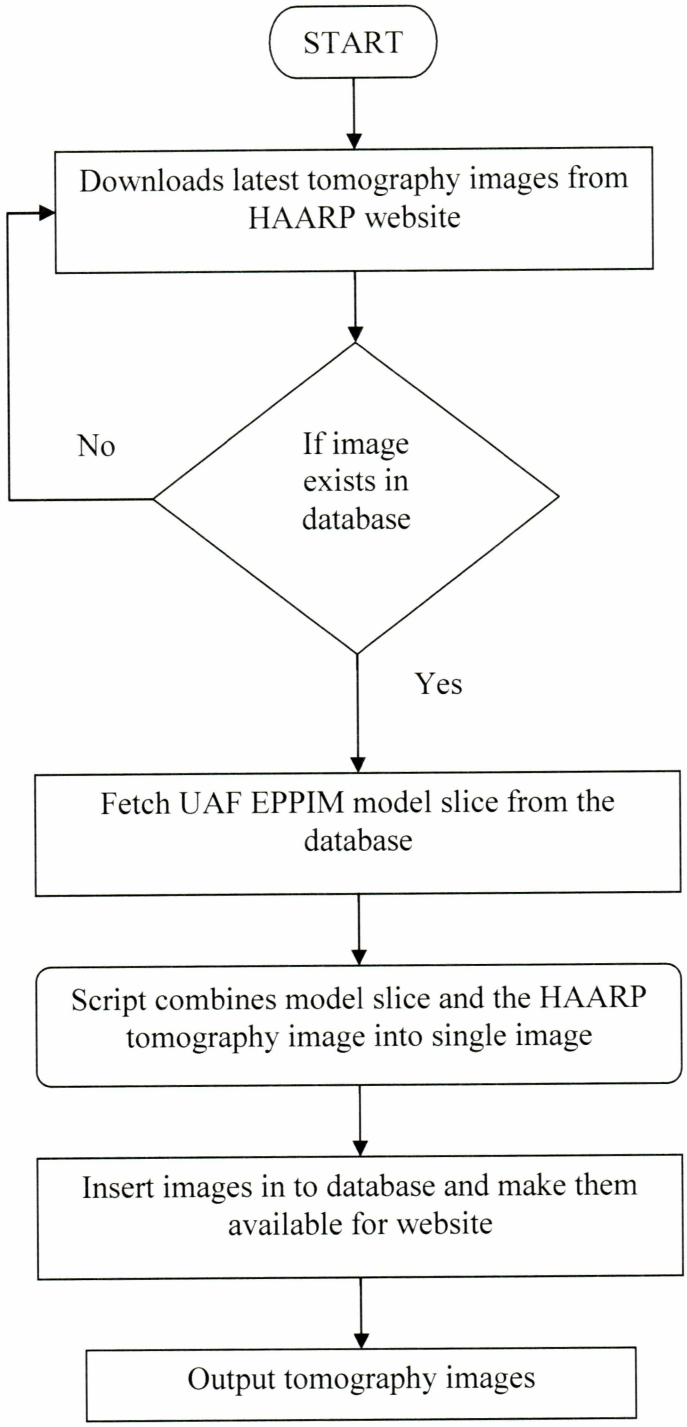

Figure 6.5 Algorithm for tomography comparisons

6.4 foF2 Comparisons

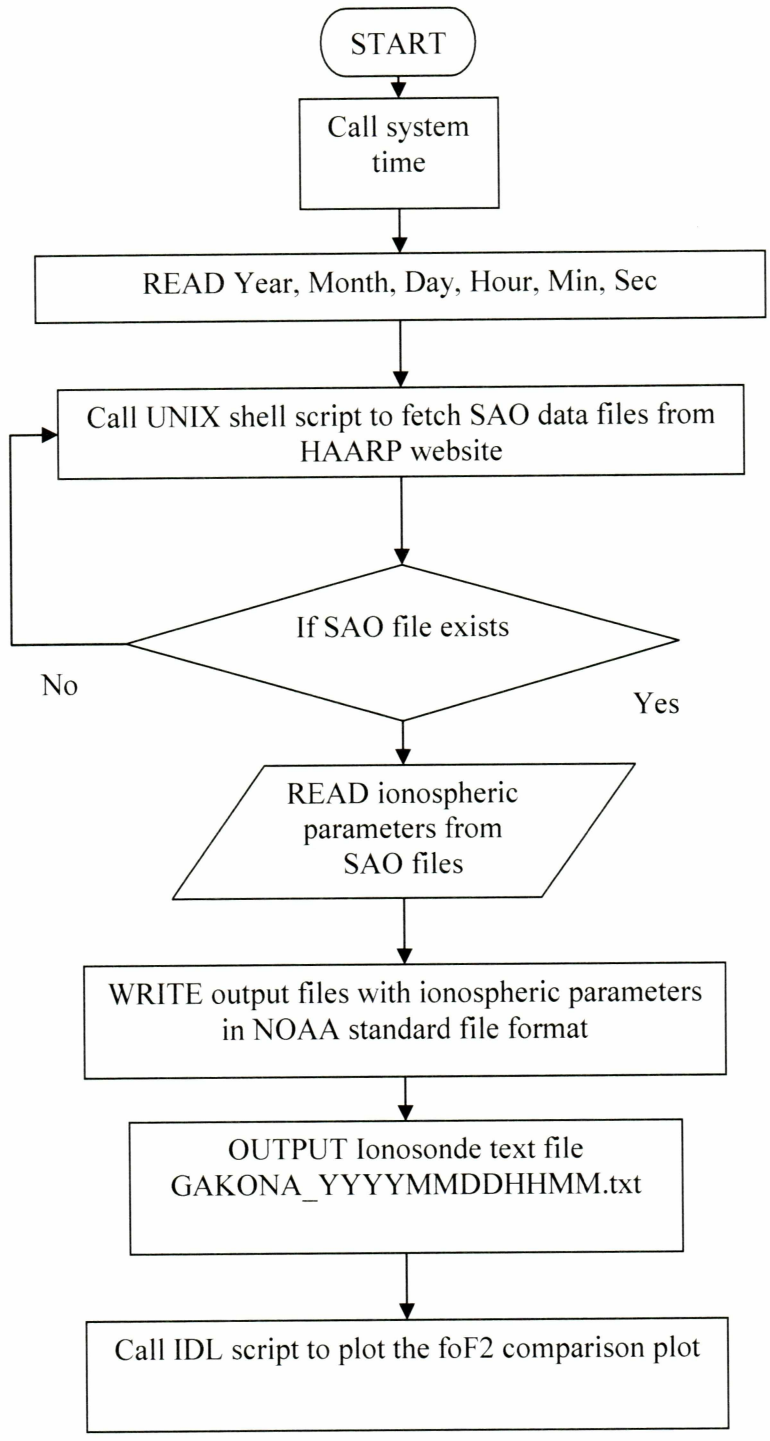

Figure 6.6 Algorithm for foF2 comparisons

Real-time Ionosonde text files are used for plotting foF2 values. Numerical emulation of the critical frequency (foF2) measurements is performed during the UAF EPPIM forecasting real-time run. The measured foF2 from a text file, and the calculated foF2 from the model, are compared in this thesis project. Code is written in FORTRAN and IDL is used for plotting the results.

This software was developed to produce ionosonde data files in the NOAA (National Oceanographic and Atmospheric Administration) standard format. We download ionosonde files, which are available in SAO format (Standard Archiving output), read the ionospheric parameters and then write those parameters into standard NOAA format. These files are used for plotting and comparing measured and model simulated foF2.

6.4.1 Call System Time

FORTRAN code initially calls the CALL SYSTEM in UNIX which gives the standard universal time; it gives current year, month, day number, hours, minutes and seconds. It is very important to know the UT time as the software fetches measured data files and does comparisons in real-time.

6.4.2 UNIX Shell Script lynx_call

The shell script lynx_call is used to fetch the digisonde data files *(GA762_2006045.SAO)* from the HAARP website that are continuously available. This

script uses the UNIX utility *lynx* to download files from the web server. These digisonde data files are downloaded in real-time and stored in the directory. The script also checks for the latest files in the directory. If the file is already downloaded then it doesn't fetch that file.

6.4.3 READ Ionospheric Parameters from SAO Files

FORTRAN code opens the SAO text files and reads the ionospheric parameters as character strings (Format A80). Some of the ionospheric parameters are foF2, foF1, foE.

6.4.4 WRITE Ionospheric Parameters in NOAA Standard Format

This program writes the output files in standard NOAA format. A sample generated file is shown in Appendix A. These files are developed on daily and monthly basis.

6.4.5 IDL Program to Plot foF2

An IDL program has been developed to plot the measured foF2 ionosonde data and simulated (UAF EPPIM) foF2 from the ionospheric model. Plots are shown in Figure 3.2 of Chapter 3.

Chapter 7 Summary, Conclusions, and Future Work

7.1 Summary and Conclusions

The work of this thesis was to develop new software tools to use experimental data to validate the UAF ionospheric model. To accomplish this goal, ionospheric data acquired at the HAARP site at Gakona, Alaska have been utilized.

First, ionosonde data were used to compare peak F-region ionospheric densities with model results. Second, integrated column abundances of ionization (total electron densities, TEC) have been derived from the model outputs and compared with experimentally derived TEC values from GPS data. To accomplish this latter task, software has been developed that accounts for real-time geometrical effects in determining the GPS satellite positions and hence make appropriate TEC determinations from the GPS data.

The plots obtained from this algorithm demonstrate the validation capability of the UAF EPPIM model. TEC, S_4, and elevation curves are similar to measured curves for data acquired from the HAARP site. Thus, measured and simulated parameters are compared and appear to be similar.

The other part of this project is to develop ionospheric tomography simulations to validate the UAF EPPIM model. Ionospheric tomography simulations are performed

using 3-D inputs of electron density from the UAF EPPIM. The Tomography reconstruction algorithm has been applied to TEC data collected by a chain of receivers in Alaska and the resulting electron density images were compared with nearly simultaneous independent measurements made by the HAARP station. The agreement observed indicates that the technique can be developed enough to be a useful tool for investigating ionospheric structures.

Tomography images are obtained in real-time from the software we developed and compared with tomography images obtained from the HAARP website. These results provide tools for validating the UAF EPPIM model.

Summarizing the software developed:

- Software was developed to produce Cartesian coordinates (position) of the individual GPS satellites from SP3 format data in real-time.
- These coordinates were then used to determine the elevation and azimuth angle of each GPS satellite.
- A function which determines the GPS time was developed.
- By knowing the position and time of each GPS satellite, total electron content (TEC) was estimated, which was compared with measured ionospheric data from the HAARP site, Gakona, Alaska.
- Software was developed to determine Low Earth Orbits satellite position.
- A script which downloads the latest real-time images from the HAARP website was developed.

- A program that produces plots of ionospheric tomography data was developed. Model generated images and images derived from downloaded data were compared.

7.2 Future Work

This software calculates and compares results for Gakona station, Alaska (HAARP). It can be extended to calculate and compare results for other locations. HAARP website provides access to data from various stations in Alaska, so our next version of this model can be improved to calculate TEC at those other stations.

TEC and scintillation parameters can be calculated by considering the Low Earth Orbit Satellites, or in other words, low flying satellites. These satellites fly at an altitude of around 1000 km (for example NNSS, FEDSAT). Low Earth Orbit Satellites provide capability for satellite-to-satellite occultation experiments to reconstruct the vertical profile of the ionosphere. Software can be developed along similar lines as we developed for GPS Satellites TEC estimation.

Satellite prediction software is in development which can predict the positions of Low Flying Satellites. This software takes the input from NORAD's two - line elements, which is available from their website and updated every hour. Thus, Satellite latitude, longitude and elevation/azimuth angles are available as outputs. These positions can be used to determine the TEC and scintillation parameters as we have determined GPS TEC

parameters in this study discussed in section 6.2. Comparison plots like Figures 4.5(a) – 4.5(e) can be obtained for Low Earth Orbit Satellites. As a test of accuracy, plots and results obtained from GPS TEC and LEO TEC can be studied further to prove the stability of the model.

References

Al'Pert, L.Y., Radio Wave Propagation and the Ionosphere, Volume 2, 1974.

Austen, J.R., S.J. Franke, C.H. Liu, Ionospheric Imaging using Computerized Tomography, Radio Science, Vol. 23(1), pp. 199-207, 1998.

Austen, J.R., T.D. Raymund, C.H. Liu, S.J. Franke, J.A. Klobuchar, and J. Stalker, Computerized ionospheric tomography, Proc. Ionospheric Effects Symposium, Springfield, VA, May 1990.

Beutler, G., Extracting Information Concerning the Ionosphere using the IGS Network, EOS Transactions of the American Geophysical Union, Vol. 76, No. 17, pp. 86., 1995.

Daniell, R.E., L.D. Brown, D.N. Anderson, M.W. Fox, P.H. Doherty, D.T. Decker, J.J. Sojka, and R.W. Schunk., Parameterized Ionospheric Model: A Global Ionospheric Parameterization Based on First Principle Models, Radio Science, Vol. 30(5), pp. 1499-1510. 1995.

Fernandez, M., Contributions to the 3D Ionospheric sounding with GPS data, PhD dissertation, Research group of Astronomy and Geomatics, University of Politecnica de Catalunya, Spain, 2004.

Fleming, H.E., Satellite Remote Sensing by the Technique of Computed Tomography, Journal of Applied Meteorology., pg 21, 1538-1549, 1982.

Fremouw, E.J., J.A. Secan, and B.M. Howe, Application of Stochastic Inverse Theory to Ionospheric Tomography, Radio Science., Vol. 27(5), 721-732, 1992.

Gherm, V. E., N. N. Zernov, and H. J. Strangeways (2005), HF Propagation in a Wideband Ionospheric Fluctuating Reflection Channel: Physically Based Software Simulator of the Channel, Radio Sci., 40, RS1001, doi:10.1029/2004RS003093.

Hargreaves, J.K, R.D. Hunsucker, The High-latitude Ionosphere and its Effects on Radio Propagation, Cambridge University, 1992.

Hofmann, B., H. Lichtenegger, Global Positioning Systems: Theory and applications, Springer-Verlag, 1997.

Klobuchar, I.A., and C.L. Rino, Trans-ionospheric Propagation Measurements using Signals from the GPS Satellites, *Proc*. International Symposium on Beacon Satellite Studies of the Earth's Environment, 505-509, New Delhi, India, 1983.

Komjathy, A., Global Ionospheric Total Electron Content Mapping using the Global Positioning System, Ph.D thesis, The University of New Brunswick, 1997.

Lanyi, G.E. and T. Roth, A Comparison of Mapped and Measured Total Ionospheric Electron Content Using Global Positioning System and Beacon Satellite Observations. Radio Science, Vol. 23(4), pp. 483-492, 1988.

Lettinger, R., G.K. Hartmann, F.I. Lohmar, and E. Putz, Electron Content Measurements with Geodetic Doppler Receivers, Radio Sei., 19(3), 789-797, 1984.

Lettinger, R., G. Schmidt, and A. Taurianien, An Evaluation Method Combining the Differential Doppler Measurements from Two Stations that Enables the Calculation of the Electron Content of the Ionosphere, Journal of Geophysics, Vol. 41, pp. 201-213, 1975.

Lewitt, RM., Reconstruction Algorithms: Transform Methods, Proc. IEEE, 71(3), 390-408, 1983.

Maurits S., Modeling of the Polar Ionosphere in the Inertial Corotating Frame, Master's thesis, University of Alaska Fairbanks, 1996.

Na, H., Tomographic Reconstruction Techniques for Imaging Electron Density Profiles in the Ionosphere, Ph.D. thesis, University of Illinois at Urbana-Champaign, Department of ECE, Urbana, IL 61801, 1991.

Parkinson, B.W., J.J. Spilker, The Global Positioning System: Theory and Applications, American Institute of Aeronautics and Astronautics, 1996.

Raymund, T.D., Application of Computerized Tomography to the Investigation of Ionospheric Structures, Master's thesis, University of Illinois at Urbana-Champaign, 1990.

Sardon, E., N. Jakowski, and N. Zarraoa, Permanent Monitoring of TEC using GPS Data: Scientific and Practical Aspects, EOS Transactions of the American Geophysical Union, Vol. 76(17), p.87, 1995.

Wang L., Mapping and Predicting the Ionospheric Effects to Communication Systems in Northern Aurora Areas using the Global Positioning System, Master's thesis, University of Alaska Fairbanks, 2002.

APPENDIX NOAA Format Data File

This is the sample text file generated from the software developed for foF2 comparisons.

200507_Gakona_iono - Notepad

File Edit Format Help

```
:Product:Gakona_iono.txt
:Issued: 2005 Nov 29 0055 UTC
#Prepared using SAO Format Filefrom HAARP Digisonde Database
#Please send comments and suggestions to kotipall@arsc.edu
#
# Units forfoF2,MUF(D),foEs,foE,fMUF, foF1, fxI & fbEs = MHz
# Units for yF2, D, hmE, hF, h & hmF2 = km
# Units for TEC = 10^16 el/m^2
# Missing dataa: -1.0, -1,-1.00
#
#    Real-Time Ionosonde Data
#    Gakona 145.3W63.2N University of Alaska Fairbanks-DYNASONDE
#
# UT Date Time
# YR MO DA  HHMM     foF2   hmF2 M(D)    D   hF  yF2 fMUF    h   fxI foF1 foE  hmE foEs fbEs  ITEC
#-------------------------------------------------------------------------------------------------
2005 07 01  0015      5.3   -1  3.05   -1   -1   -1  4.9    0   6.1  4.3  3.1   -1  3.1  0.0   8.7
2005 07 01  0030      5.2   -1  3.04   -1   -1   -1  4.8    0   6.1  4.3  3.1   -1  3.3  0.0   9.1
2005 07 01  0045      5.2   -1  3.06   -1   -1   -1  4.9    0   6.1  4.4  2.8   -1  3.1  0.0   9.3
2005 07 01  0100      5.4   -1  3.26   -1   -1   -1  5.1    0   6.2  4.3  2.9   -1  3.0  0.0   8.1
2005 07 01  0115      5.3   -1  3.06   -1   -1   -1  4.8    0   6.1  4.2  3.0   -1  3.0  0.0  10.3
2005 07 01  0130      5.2   -1  3.17   -1   -1   -1  5.0    0   6.0  4.3  2.9   -1  4.9  0.0   7.8
2005 07 01  0145      5.0   -1  3.11   -1   -1   -1  4.7    0   5.9  4.2  2.8   -1  2.8  0.0   7.3
2005 07 01  0200      5.1   -1  3.04   -1   -1   -1  5.0    0   6.0  4.3  2.9   -1  2.8  0.0   8.4
2005 07 01  0215      4.9   -1  3.22   -1   -1   -1  4.7    0   5.9  4.2  2.7   -1  2.8  0.0   6.9
2005 07 01  0230      5.1   -1  3.03   -1   -1   -1  4.7    0   6.0  4.1  2.5   -1  2.7  0.0   8.7
2005 07 01  0245      5.1   -1  3.08   -1   -1   -1  4.8    0   5.9  4.1  2.6   -1  2.6  0.0   8.1
2005 07 01  0300      4.9   -1  3.14   -1   -1   -1  4.6    0   5.9  4.0  2.6   -1  2.6  0.0   7.5
2005 07 01  0315      5.2   -1  3.02   -1   -1   -1  4.8    0   6.0  3.9  2.5   -1  5.6  0.0   8.8
2005 07 01  0330      5.3   -1  3.23   -1   -1   -1  4.9    0   6.1  3.9  2.4   -1  2.4  0.0   7.6
2005 07 01  0345      5.1   -1  3.20   -1   -1   -1  4.7    0   5.9  3.8  2.2   -1  2.3  0.0   6.7
2005 07 01  0400      4.9   -1  3.19   -1   -1   -1  4.6    0   5.8  3.7  2.3   -1  2.9  0.0   6.2
2005 07 01  0415      4.9   -1  3.19   -1   -1   -1  4.7    0   5.8 -1.0  2.3   -1  3.0  0.0   6.3
2005 07 01  0430      5.2   -1  2.99   -1   -1   -1  4.6    0   6.1 -1.0  2.3   -1  2.9  0.0   9.5
2005 07 01  0445      5.3   -1  3.26   -1   -1   -1  5.0    0   6.2  3.4  2.1   -1  2.8  0.0   7.3
2005 07 01  0500      5.3   -1  3.17   -1   -1   -1  5.0    0   6.1  3.2  2.1   -1  2.4  0.0   6.6
2005 07 01  0515      5.4   -1  3.32   -1   -1   -1  5.1    0   6.2  3.1  2.1   -1  3.0  0.0   5.6
2005 07 01  0530      5.2   -1  3.10   -1   -1   -1  4.6    0   6.1  3.0  2.0   -1  3.7  0.0   7.5
2005 07 01  0545      5.5   -1  3.24   -1   -1   -1  5.1    0   6.3  2.8  1.9   -1  3.3  0.0   7.0
2005 07 01  0600      5.2   -1  3.46   -1   -1   -1  5.0    0   6.1  2.7  1.8   -1  3.7  0.0   4.5
2005 07 01  0615      5.3   -1  3.33   -1   -1   -1  5.0    0   6.2 -1.0  1.7   -1  3.9  0.0   6.2
2005 07 01  0630      5.2   -1  3.39   -1   -1   -1  4.9    0   6.1 -1.0  1.6   -1  4.6  0.0   5.6
2005 07 01  0645      4.9   -1  3.38   -1   -1   -1  4.6    0   6.1 -1.0  1.5   -1  2.6  0.0   4.8
2005 07 01  0700      4.8   -1  3.33   -1   -1   -1  4.4    0   5.9 -1.0  1.5   -1  2.6  0.0   4.6
2005 07 01  0715      4.6   -1  3.41   -1   -1   -1  4.2    0   5.8 -1.0 -1.0   -1  2.8  0.0   3.4
2005 07 01  0745      3.9   -1  3.38   -1   -1   -1  3.5    0   4.7 -1.0 -1.0   -1 -1.0  0.0   3.0
2005 07 01  0800      3.8   -1  3.13   -1   -1   -1  3.4    0   4.7 -1.0 -1.0   -1 -1.0  0.0   3.3
2005 07 01  0815      3.8   -1  2.97   -1   -1   -1  3.4    0   4.6 -1.0 -1.0   -1 -1.0  0.0   3.8
2005 07 01  0830      3.8   -1  3.01   -1   -1   -1  3.5    0   4.7 -1.0 -1.0   -1 -1.0  0.0   3.6
2005 07 01  0845      3.7   -1  3.04   -1   -1   -1  3.3    0   4.5 -1.0 -1.0   -1 -1.0  0.0   2.9
2005 07 01  0900      3.7   -1  3.16   -1   -1   -1  3.3    0   4.6 -1.0 -1.0   -1 -1.0  0.0   2.7
2005 07 01  0915      3.4   -1  2.99   -1   -1   -1  3.0    0   4.2 -1.0 -1.0   -1 -1.0  0.0   2.8
2005 07 01  0930      3.3   -1  3.09   -1   -1   -1  3.0    0   4.2 -1.0 -1.0   -1 -1.0  0.0   2.2
2005 07 01  0945      3.3   -1  3.11   -1   -1   -1  3.0    0   4.1 -1.0 -1.0   -1 -1.0  0.0   2.2
2005 07 01  1015      3.2   -1  2.93   -1   -1   -1  3.0    0   4.0 -1.0 -1.0   -1  2.0  0.0   2.7
2005 07 01  1030      3.2   -1  3.05   -1   -1   -1  2.9    0   4.0 -1.0 -1.0   -1  1.8  0.0   2.3
2005 07 01  1045      3.1   -1  3.20   -1   -1   -1  2.9    0   4.0 -1.0 -1.0   -1  2.6  0.0   1.8
2005 07 01  1100      3.0   -1  3.49   -1   -1   -1  3.0    0   4.0 -1.0 -1.0   -1  2.9  0.0   1.2
2005 07 01  1115      3.0   -1  3.04   -1   -1   -1  2.8    0   4.0 -1.0 -1.0   -1  2.7  0.0   2.4
2005 07 01  1130      3.4   -1  2.97   -1   -1   -1  3.2    0   4.3 -1.0 -1.0   -1  3.0  0.0   2.8
2005 07 01  1145      3.2   -1  3.15   -1   -1   -1  2.8    0   4.0 -1.0 -1.0   -1  2.9  0.0   2.4
2005 07 01  1200      3.6   -1  2.83   -1   -1   -1  3.2    0   4.7 -1.0 -1.0   -1  2.9  0.0   4.2
```